

Variability of the thermohaline structure and transport of Atlantic water in the Arctic Ocean based on NABOS hydrography data

Nataliya Zhurbas¹ and Natalia Kuzmina¹

5 ¹Shirshov Institute of Oceanology, Russian Academy of Sciences, 36 Nakhimovsky Prospekt ,
117997 Moscow, Russia

Correspondence to: Nataliya Zhurbas (nvzhurbas@gmail.com)

Abstract. Conductivity-temperature-depth (CTD) transects across continental slope of the Eurasian Basin and the St. Anna Trough performed during NABOS (Nansen and Amundsen
10 Basins Observing System) project in 2002–2015 and a transect from the Polarstern-1996 expedition are used to describe the temperature and salinity characteristics and volume flow rates of the current carrying the Atlantic Water (AW) in the Arctic Ocean. The variability of the AW on its pathway along the slope of Eurasian Basin is investigated. A dynamic Fram Strait branch of the Atlantic Water (FSBW) is identified on all transects, including two transects in the
15 Makarov Basin (along 159°E), while the cold waters on the eastern transects along 126°E, 142°E and 159°E , which can be associated with the influence of the Barents Sea branch of the Atlantic water (BSBW), were observed in the depth range below 800 m and had a negligible effect on the spatial structure of isopycnic surfaces. The geostrophic volume transport of AW decreases farther away from the areas of the AW inflow to the Eurasian Basin, decreasing by one order of
20 magnitude in the Makarov Basin at 159°E, implying that the major part of the AW entering the Arctic Ocean circulates cyclonically within the Nansen and Amundsen Basins. There is an absolute maximum of θ_{max} (AW core temperature) in 2006–2008 time series and a maximum in 2013, but only at 103°E. Salinity $S(\theta_{max})$ (AW core salinity) time series display an increase of the AW salinity in 2006–2008 and 2013 (at 103°E) that can be referred to as a AW salinization in
25 the early 2000s. The maxima of θ_{max} and $S(\theta_{max})$ in 2006 and 2013 are accompanied by the volume transport maxima. The time average geostrophic volume transports of AW are 0.5 Sv in the longitude range 31–92°E, 0.8 Sv in the St. Anna Trough and 1.1 Sv in the longitude range 94–107°E.

1 Introduction

30 Atlantic water (AW) enters the Eurasian Basin in two branches (see, e.g., Aagaard, 1981; Rudels et al., 1994; Schauer et al., 1997; Rudels et al., 1999; Schauer et al., 2002a, b; Rudels et al., 2006; Berzczynska-Möller et al., 2012; Rudels et al., 2015; Rudels, 2015; Dmitrenko et al.,

2015; Pnyushkov et al., 2015, 2018b): one branch originates from the Greenland and Norwegian seas and flows to the basin through Fram Strait (the Fram Strait branch of the Atlantic Water, hereinafter the FSBW), and the other reaches the deep part of the Arctic Ocean near St. Anna Trough after passing through the Barents Sea (the Barents Sea branch of the Atlantic water, hereinafter the BSBW). After entering the Eurasian Basin the FSBW moves eastward with a subsurface boundary current and has a core of higher temperature and salinity than the BSBW. In the longitude range of 80–90°E, it encounters and partially mixes with the BSBW, which is strongly cooled due to mixing with shallow waters of the Arctic shelf seas and atmospheric impact (Schauer et al., 1997; 2002a, b). Further, the water masses resulting from the interaction of the two branches spread cyclonically in the Eurasian Basin.

Within the NABOS (Nansen and Amundsen Basins Observing System) project (Polyakov et al., 2007) a unique volume of CTD data was collected: more than 30 sections were made in various regions of the Arctic Basin in the summer/fall 2002-2015. A number of sections in different years were made in the same regions of the Basin, which allows studying the interannual variability of the water masses thermohaline structure and the geostrophic volume flow rate in these areas.

The main goal of this work is to investigate the spatial and temporal variability of the AW geostrophic volume flow rate during its propagation along the continental slope of the Eurasian Basin. We further discuss the thermohaline structure and transformation of the FSBW and BSBW. The estimates of the AW transport are sensitive to the temperature and salinity ranges used for the identification of this water (Pnyushkov et al., 2018b) and mixing of FSBW, BSBW and surrounding waters may change the AW geostrophic volume flow rate.

2 Material and Methods

We used data from the CTD transects across the slope of the Eurasian Basin in the longitude range of 31–159°E measured in the years 2002–2015 within the framework of NABOS project (in total 39 transects). The data are freely available at the site <http://nabos.iarc.uaf.edu>. In addition, a CTD transect across the entire Eurasian Basin and over the Lomonosov Ridge starting at 92°E at the slope from R/V *Polarstern* in 1996 (hereafter PS96) was also included. The locations of the CTD transects are shown in Fig. 1. Most of the transects are aligned cross-slope and grouped at longitudes of 31, 60, 90, 92, 94, 96, 98, 103, 126, 142, and 159°E. Four of the 40 transects crossed zonally the St. Anna Trough (at the latitude of 81, 81.33, 81.42, and 82°N) through which the BSBW enters the Eurasian Basin. Most of the CTD casts covered the upper layer from the sea surface to either 1000 m depth or to the bottom (if the total depth was

shallower). Approximately every third or fourth cast was down to the sea bottom even if the sea depth exceeded 1000 m.

To estimate the volume transport of the Atlantic Water, we applied standard dynamical method. The no-motion level (the depth of zero velocity) was determined from the following consideration. If the baroclinic current occupies the upper layer or/and some intermediate layer, the no-motion level can be chosen in a calm deep layer (where the horizontal density gradient is relatively small). On the contrary, in case of a near-bottom gravity flow, the no motion level can be reasonably chosen well above the near-bottom flow. We adopted for the level of no-motion either 1000 m depth or the sea bottom depth if the latter was smaller than 1000 m for the FSBW, and approximately 50 m, where density contours were more or less flat, for the observations of BSBW in the St. Anna Trough (see also below).

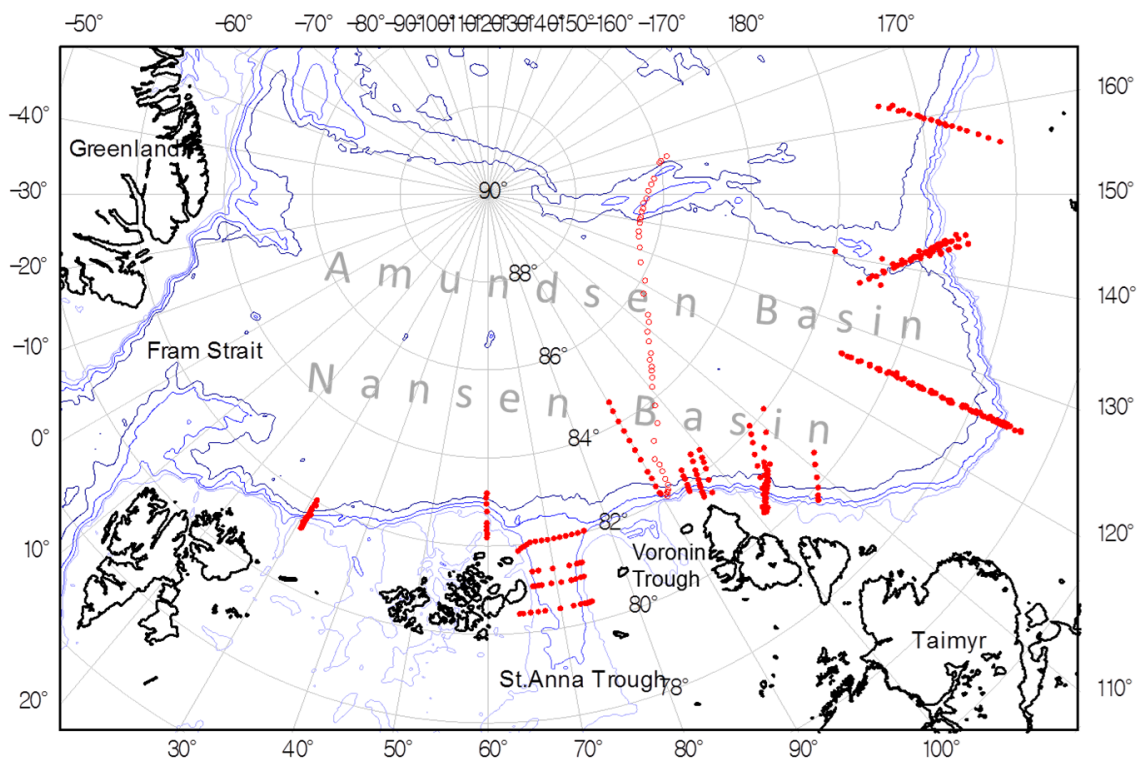


Fig. 1. Bathymetric map of the Eurasian Basin with 300, 500, 1000, and 2000 m contours shown. The red filled and blank circles are the locations of CTD stations on the NABOS and PS96 transects, respectively.

Since the FSBW brings saline and warm water to the Eurasian Basin, the geostrophic transport was found by integration over the depth range with positive temperature, $\theta > 0$ °C, and relatively high salinity, $S > 34.5$ (the salinity is given in the practical salinity scale), that is, near-surface layers with warm and fresh water (which cannot be attributed to AW) were excluded. For the observations of BSBW in the St. Anna Trough the geostrophic transport was calculated by

integration over a depth range with temperature below 0 °C and salinity above 34.5. If both AW branches were present on the transect, the integration was performed over the entire depth range but excluding the cold near-surface layer ($\theta < 0$ °C) and the warm ($\theta > 0$ °C) and relatively fresh ($S < 34.5$) near-surface layer. The zero velocity depth in this case was chosen after inspection of
 90 the observed pattern of density contours, i.e. suggesting either the near-surface flow pattern or the near-bottom flow pattern (see Section 3). The details and limitation of the geostrophic velocity calculations are discussed in Zhurbas (2019).

3. Results

3.1 Variability of the thermohaline pattern on the AW pathway along the slope of Eurasian 95 Basin

3.1.1 CTD transects analysis

The transformation of thermohaline signatures (i.e. patterns of salinity S , potential temperature θ , and potential density anomaly σ_θ , versus cross-slope distance and depth) of the AW flow on its pathway along the slope of the Eurasian Basin are presented in Fig.2. The σ_θ
 100 contours on transects at 31°E diverge towards the continental slope margin (to the south), shallowing above the warm/saline core of the AW and sloping down beneath it associated with an eastward subsurface flow. Such distribution of isopycnic surfaces was observed on all NABOS transects taken across available continental slope at 31°E. According to Fig. 2 the warm/saline core of the Fram Strait Branch of the AW with the maximum temperature θ_{max} of 4.88°C at the
 105 depth $Z_{\theta_{max}}=102$ m and the maximum salinity S_{max} of 35.11 at the depth $Z_{S_{max}}=176$ m is found on the slope at about 1000 m isobath.

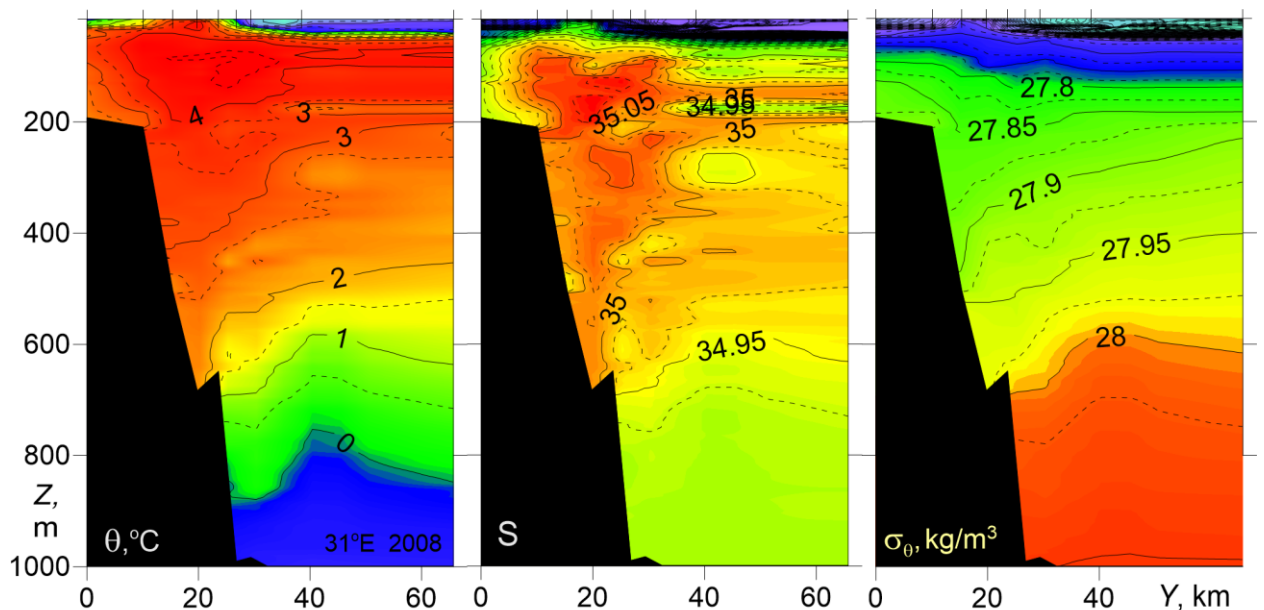


Fig. 2. Temperature θ , salinity S , and potential density anomaly σ_θ versus cross-slope distance and depth for the NABOS-2008 transect across the Eurasian Basin slope at 31°E.

110 Figure 3 presents temperature, salinity, and potential density for two zonal transects across the St. Anna Trough at latitudes of 81 and 82°N. A stable pool of cold ($\theta < 0^\circ\text{C}$) and dense ($\sigma_\theta > 28 \text{ kg/m}^3$) water in the bottom layer is seen adjacent to the eastern slope of the trough. The transfer of the densest water pool to the eastern slope corresponds to a geostrophically balanced near-bottom gravity flow to the North. This near-bottom gravity current carries also waters of
115 Atlantic origin, which are strongly cooled due to mixing with shelf waters in the Barents and Kara seas. Above the near-bottom gravity flow of the BSBW one can observe two-core structure of warm FSBW with temperature up to 2.5 °C that enters the St. Anna Trough from the north-west at the western side of the trough and leaves it for the north-east at the eastern side of the trough. At 82°N, the BSBW overflows a ridge-like elevation east of the St. Anna Trough (top
120 panels in Fig. 3). Studies of the currents and hydrography in the St. Anna Trough can be found in (Schauer et al., 2002a, b; Rudels et al., 2015; Dmitrenko et al., 2015).

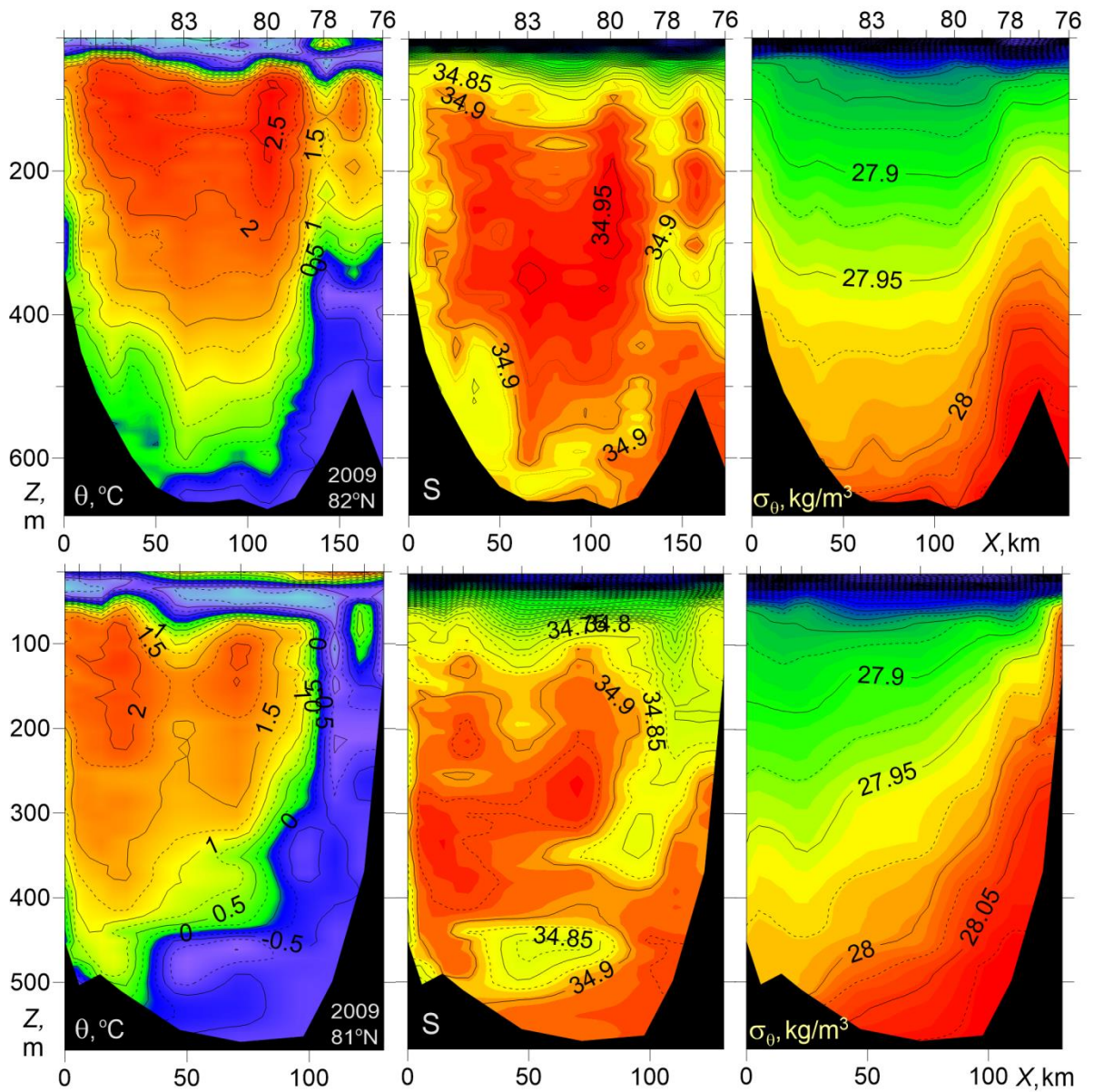


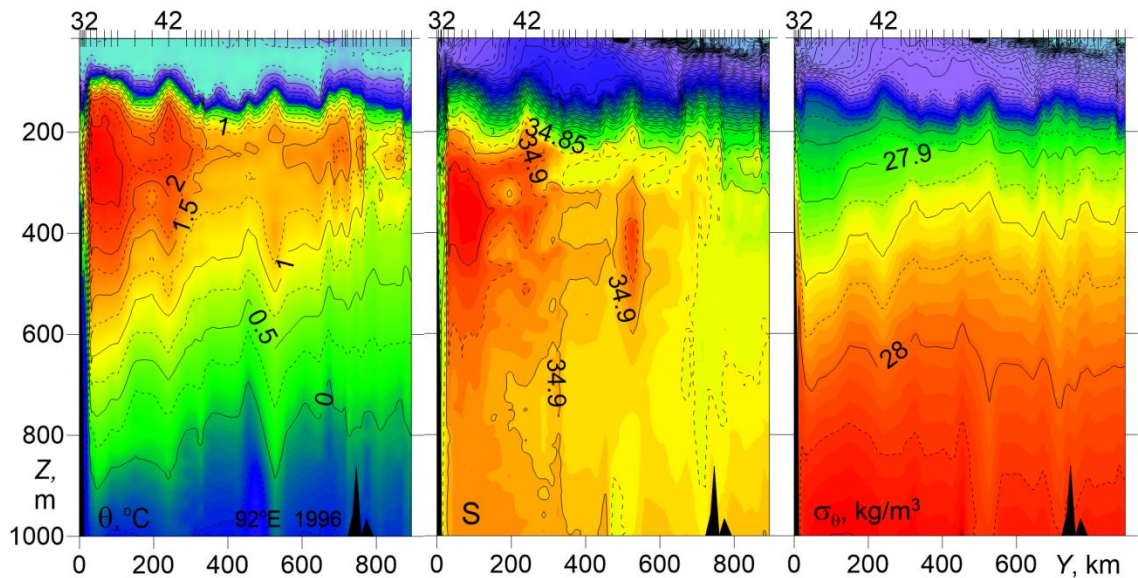
Fig. 3. Temperature θ , salinity S , and potential density anomaly σ_θ versus distance and depth for zonal transects across the St. Anna Trough at latitudes of 81°N (bottom, NABOS-2009), and 82°N (top, NABOS-2009). The X-axis is directed to the east.

In order to understand the effect of the FSBW and the BSBW transformation on geostrophic volume flow rate, it is necessary to identify water masses of different origin. For that purpose the following criterion is often used (Walsh et al., 2007; Pfirman et al., 1994): the water masses of the FSBW are characterized by $\theta > 0$ °C, and the BSBW can be identified by -2 °C $<$ $\theta < 0$ °C, $34.75 < S < 34.95$ and $27.8 \text{ kg/m}^3 < \sigma_\theta < 28.0 \text{ kg/m}^3$. Other approaches to define BSBW are given in Schauer et al. (1997; 2002a, b) and Dmitrenko et al. (2015). According to Schauer et al. (1997; 2002a, b) the BSBW includes all waters that enter the Nansen Basin from the St. Anna and Voronin troughs. The temperature of these waters, however, can reach ~ 1 °C.

135 The justification for this approach was based on θ - S analysis of the waters of the north-eastern part of the Barents Sea and the St. Anna and Voronin troughs. According to Dmitrenko et al. (2015), the BSBW consists of two water masses, and the temperature of the warmer water mass can only slightly exceed 0 °C (for more details see section 3.1.2). Here we will rely on the definitions of the FSBW and BSBW proposed by Dmitrenko et al. (2015).

140 In Fig. 4 the CTD transect at 92°E carried out in the *Polarstern*-1996 expedition just east of the entrance point of the BSBW to the Eurasian Basin from the St. Anna Trough and Voronin Trough is presented. It can be assumed that a part of the BSBW extends deep into the Basin, mixing with the FSBW, while another part of the BSBW flows eastward along the slope according to the general cyclonic circulation observed in the Eurasian Basin. On the presented
145 transect the BSBW is observed in the depth range below 600 m as a narrow, about 10 km wide strip of cold water near the slope (see also Subsection 3.1.2) adjacent to a 300 km wide zone occupied by the warm FSBW. The potential density distribution of FSBW on this transect is similar to transects at 31°E. Namely, despite of the masking effect of vertical undulations of σ_θ contours caused by internal waves and mesoscale eddies (one of subsurface, intra-pycnocline eddies is probably identified at the distance of $Y=510$ km), isopycnals tend to shoal/deepen
150 above/below the FSBW core towards the continental slope margin (to the south) which, in terms of geostrophic balance implies the eastward flow of FSBW. The FSBW core on the 92°E transect is found at 40 km distance from the slope, with the maximum temperature $\theta_{max}=2.79^\circ\text{C}$ at $Z_{\theta_{max}}=271$ m and salinity $S_{max}=34.97$ at $Z_{S_{max}}=329$ m. Therefore, the FSBW on its pathway
155 along the slope of the Eurasian Basin from 31°E to 92°E has cooled, desalinated, sank and become denser by about 2 °C, 0.1, 150 m, and 0.1 kg/m³, respectively. Another distinct feature in the PS96 transect is a layer with increased temperature between 180 and 300 m depth at $Y=600$ – 750 km in the vicinity of the Lomonosov Ridge, which can be attributed to the geostrophically-balanced FSBW return flow cyclonically circulating around the Eurasian Basin (Rudels et al.,
160 1994; Swift et al., 1997).

According to Schauer et al. (2002b) who studied the PS-96 section, the horizontal and vertical scales of the BSBW were taken at 30 km and 800 m, respectively. This differs from our interpretation based on the definition of BSBW with temperature less than 0 °C.



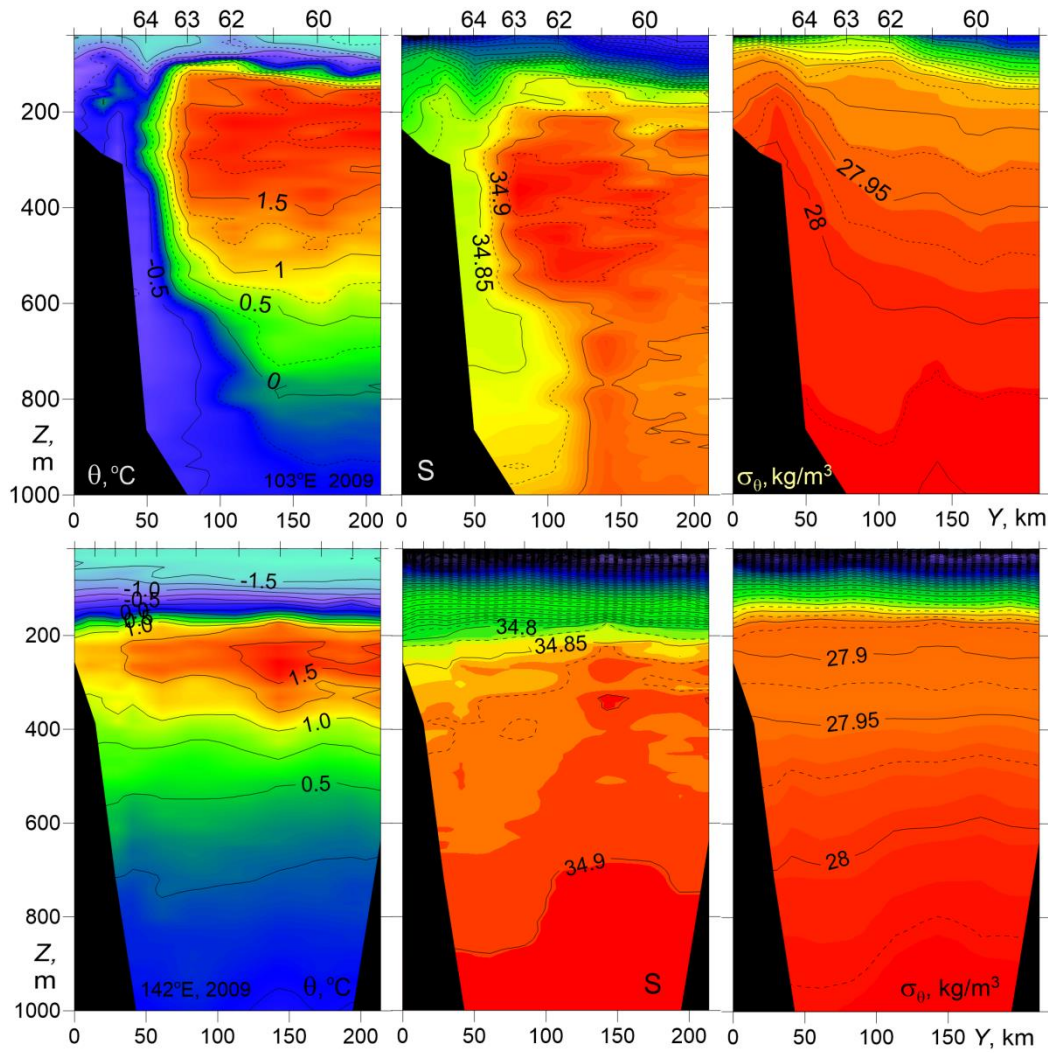
165 Fig. 4. Temperature θ , salinity S , and potential density anomaly σ_θ versus distance and depth for cross-shelf transects at 92°E (PS-1996).

Further east, in the longitude range of 94–107 °E (NABOS-09), the denser part of BSBW under the FSBW is characterized by an eastward geostrophic current with isopycnals sloping towards the North in a 150 km wide zone adjacent to the slope (see Fig. 5, top panel). Less saline water at the slope is the less dense BSBW that has entered the Nansen Basin when the slope narrows north of Severnaya Zemlya (Schauer et al., 1997).

The vertical location of the FSBW layer is similar to the 92°E in the section PS-96 but the maximum temperature has further decreased: in the transect in Fig. 5, the top panel, $\theta_{max}=1.98$ °C at $Z_{\theta_{max}}=245$ m and $S_{max}=34.95$ at $Z_{S_{max}}=365$ m. The bottom panel of Fig. 5 presents the transect at 142°E (NABOS-09) which is located on the Lomonosov Ridge, between the Amundsen and Makarov Basins. The comparison of the two transects obtained in the same year shows that the vertical scale of the warm FSBW water ($\theta>1.5$ °C) has significantly decreased. Nevertheless, the FSBW waters are also observed at this longitude and affect the slopes of isopycnic surfaces in a layer up to 300 m. The cold waters with $\theta<0$ °C, which can be associated with the BSBW, are observed only at two stations in the depth range close to 1000 m, and are absent at depths above 950 m. The isopycnic surfaces in the bottom panel of Fig. 5 are relatively flat, indicating weak geostrophic flow (see Section 3.2). The “absolutely stable” thermohaline stratification below the temperature maximum with temperature decreasing and salinity increasing with depth (Fig. 5, bottom panel) is common to the Upper Polar Deep Water (UPDW) layer (Rudels et al., 1999).

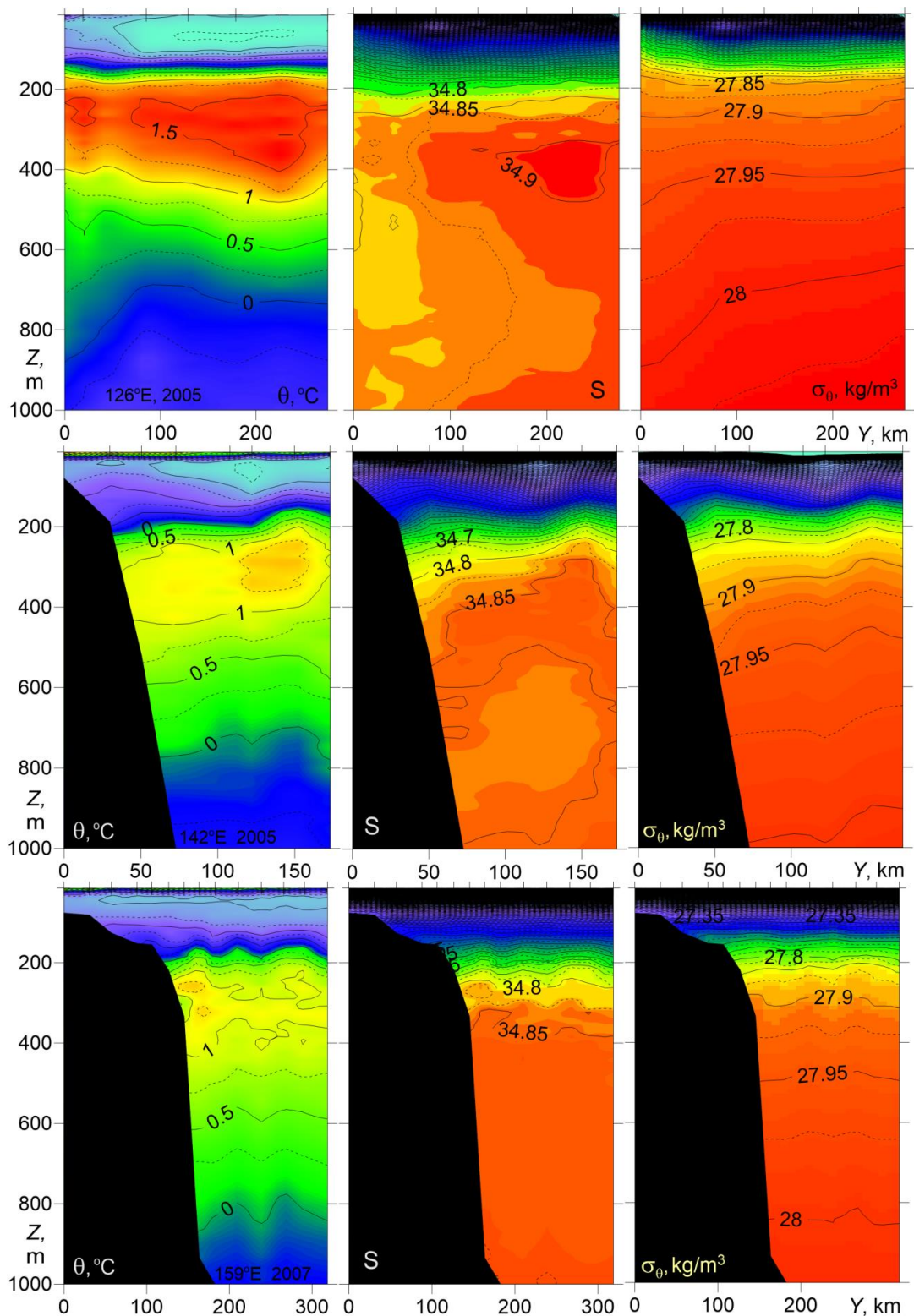
In Fig. 6 three transects are presented, at 126°E and 142°E (NABOS-2005) and in the Makarov Basin at 159° E (NABOS-2007). On the transect along 126°E large slopes of isopycnic

surfaces are observed, which corresponds to a fairly strong geostrophic flow (see Section 3.2), confined to the depth range of 200–400 m, that is, to the area occupied by the FSBW. At the 142°E transect on the Lomonosov Ridge, and at the 159°E transect in the Makarov Basin, the FSBW can be still identified as a warm layer between 200 and 400 m, where the maximum temperature is reduced to 1.49 °C and 1.42 °C, respectively (Fig. 6). The 142°E transect implies some eastward geostrophic transport, whereas at the 159° E transect, and in the area of cold waters (below 800 m) in the sections shown in Fig. 6, the baroclinic flow is weak or absent.



195

Fig. 5. Temperature θ , salinity S , and potential density anomaly σ_θ versus distance and depth for cross-shelf transects at 103°E (upper) and 142°E (lower) (NABOS-09).



200 Fig. 6. Temperature θ , salinity S , and potential density anomaly σ_θ versus distance and depth for cross-shelf transects at 126°E, 142°E (top and middle, NABOS-2005) and 159°E (bottom, NABOS-2007).

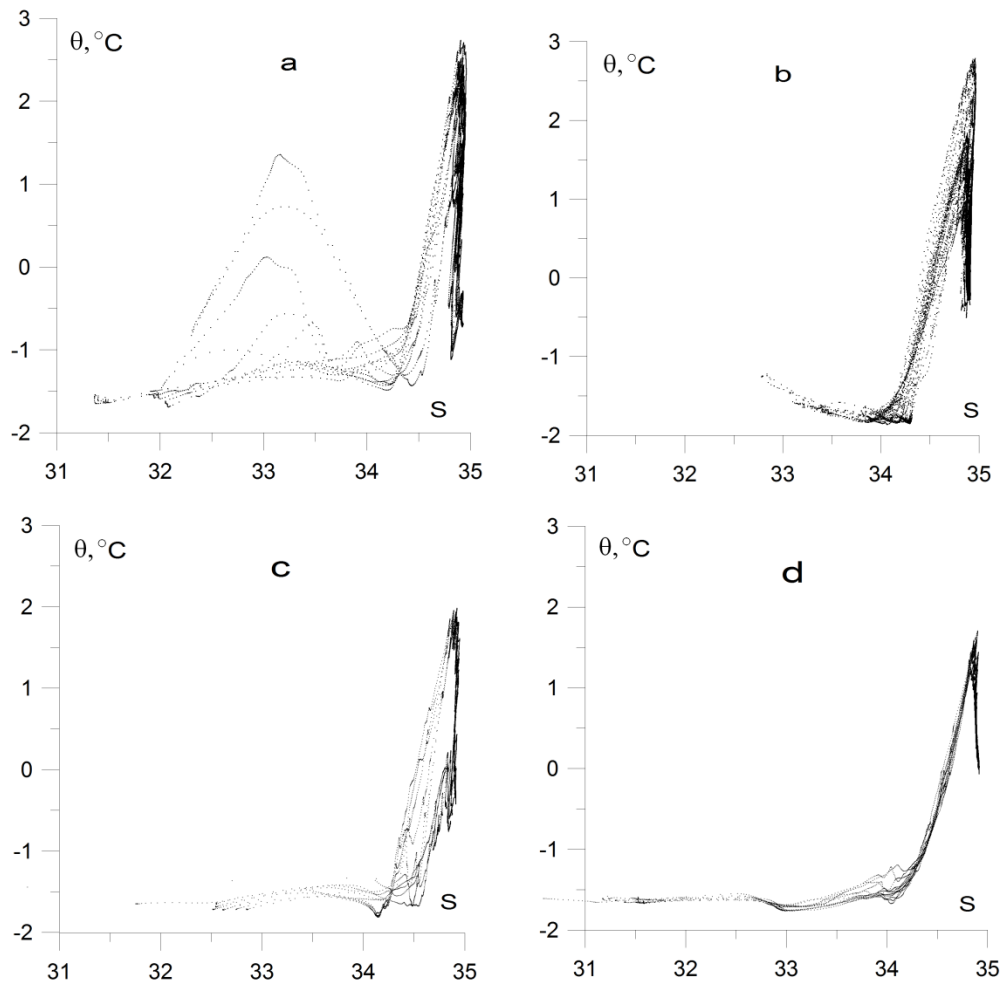
In summary, a combined FSBW-BSBW structure with isopycnals sloping down to the north (from the slope), is typical for the longitude range 94–107°E. In the transects along 126°E,
 205 142°E, and 159°E, sloping isopycnals were observed generally in the depth range of 200–400 m,

that is in the area occupied by the FSBW. As the FSBW moved along the continental slope of the Eurasian Basin, its core temperature decreased, but could be identified at all transects, including the two transects in the Makarov Basin (159°E). The cold waters in the transects along 126°E, 142°E and 159°E, which can be associated with the BSBW, had a minimum temperature above -0.5 °C, were located below 800 m, and had relatively flat isopycnic surfaces.

3.1.2 θ - S analysis

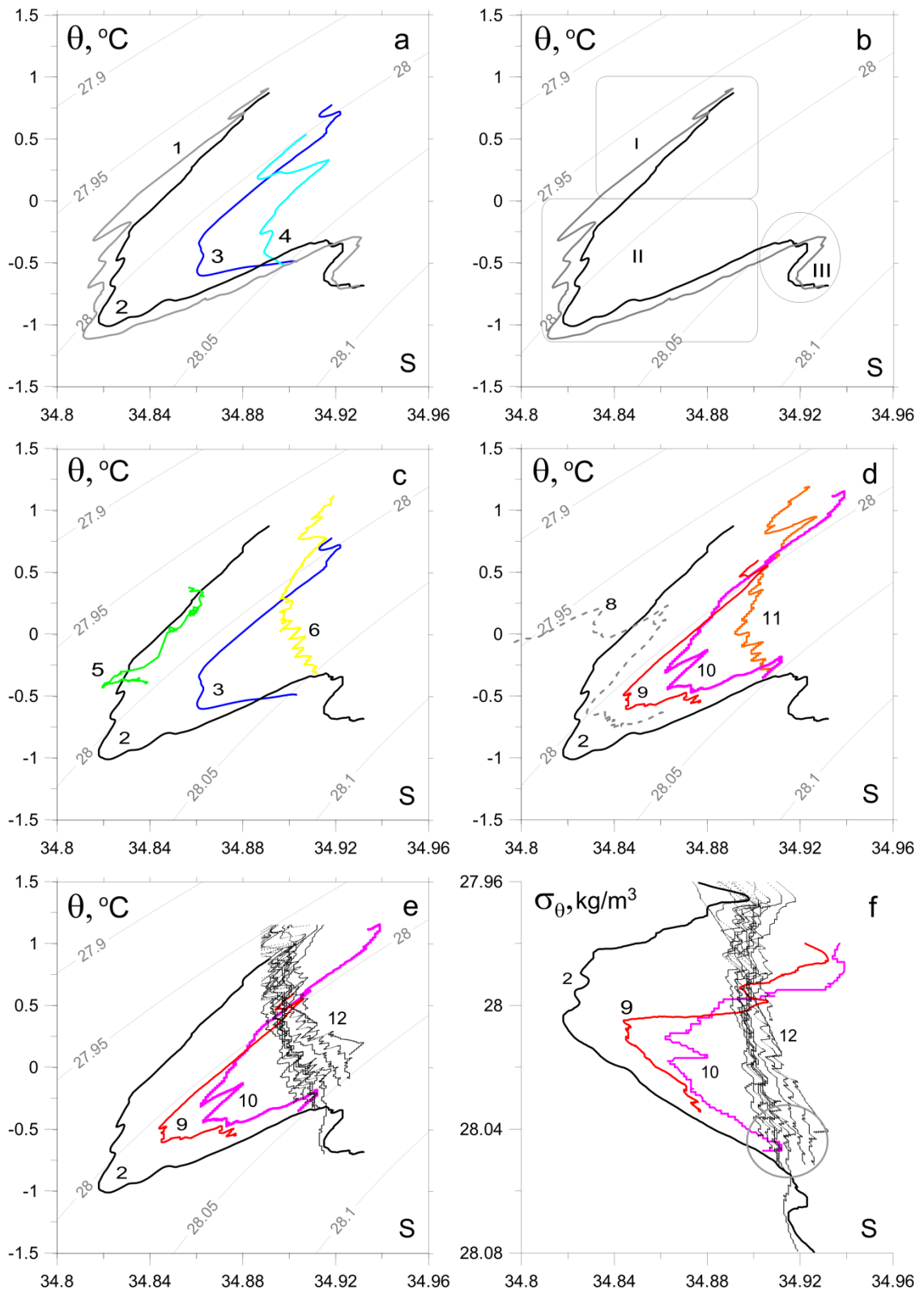
The difficulty in identifying the BSBW in the eastern part of the Nansen Basin is related to the overlapping ranges of temperature and salinity inherent to the BSBW and the UPDW: -0.5 °C $< \theta < 0$ °C, and the salinity is close to 34.9 (Rudels et al., 1994; Walsh et al., 2007). It is also important to note that the BSBW in the St. Anna Trough mixes with the FSBW. Therefore, not only the cold Atlantic Waters, which are transported by the bottom gravity current, but also mixed warmer waters can enter the Nansen Basin through the trough (see Fig. 3). A detailed θ - S analysis of different CTD sections can provide useful information on the transport and transformation of FSBW and BSBW. A distinct θ - S signature indicates that the water mass has entered the area of observation. The absence of a signature on the theta- S space indicates either the water mass did not enter the area of observation or was transformed after mixing with other waters.

The differences in the behavior of the θ - S values are observed in the upper and deep layers of the Eurasian Basin and the St. Anna Trough (Fig.7). On the other hand, one cannot miss a similarity in the shape of the θ - S curves in the salinity range of 34.5–35.0. The similarity is obviously caused by the presence of FSBW. Fig. 7 demonstrates the transformation of the FSBW and BSBW moving along the continental slope of the Eurasian Basin. More detailed information on the BSBW transformation can be extracted from θ - S diagrams presented in Fig. 8.



230

Fig. 7. θ - S diagrams based on the CTD profiling in (a) the St. Anna Trough (NABOS-09, 82° N), (b) the PS-96 section at 92°E, and the NABOS-09 sections at 103°E (c) and 142°E (d). For convenience of presentation, the points of the θ - S curves with salinity below 30 were excluded.



235 Fig. 8. Thermohaline values of the BSBW and FSBW: a) based upon the CTD profiles, obtained
 in the St. Anna Trough (NABOS-09, section 82°N), curves 1–4 correspond to the stations (st.)
 76, 78, 83 and 80, respectively; b) the same as “a” but only curves 1 and 2 are presented; regions
 I, II, III illustrate three different water masses in accordance with (Dmitrenko et al., 2015); for
 explanation see the text; c) based upon the section of PS-96, curves 5 and 6 corresponding to st.
 240 32 and 42, respectively (depth range 600–1000 m), curves 2 and 3 are shown for the reference;

d) for CTD profiles at the 103°E section, NABOS-09, curve 8 (st. 64), curve 9 (st. 63), curve 10 (st. 62), curve 11 (st. 60), and curve 2 for the reference (see Fig. 5 for the location of the stations); e) based upon the CTD profiles in the depth range 500–1200 m measured at the 126°E (section of NABOS-09), curves 12; curves 2, 9 and 10 are shown for the reference; f) the same as “e” but presented in coordinates σ_θ, S .

The θ - S curves marked as 1 and 2 in Fig.8a correspond to stations 76 and 78, respectively, which were located at the eastern slope of the St. Anna Trough just in the near-bottom gravity current carrying the BSBW, while the curves marked as 3 and 4 correspond to stations 83 and 80 located near the mid-point (thalweg) of the trough in the western periphery of the gravity current (the location of the stations is shown in Fig. 3). To visualize the BSBW transformation better, the points of θ - S curves in the temperature and salinity ranges of $\theta > 1.2$ °C and $S < 34.76$, respectively, were omitted. Similar θ - S curves in the St. Anna Trough were observed within NABOS Program in other years (NABOS-13, NABOS-15).

The curves 1 and 2 in Fig. 8a have similar knee-like shape (Dmitrenko et al., 2015) formed by (i) the upper warm and saline water layer of the FSBW ($\theta \gg 0$ °C), (ii) the intermediate colder and fresher water layer of BSBW ($\theta < 0$ °C) underlying the FSBW, and (iii) the denser, warmer and saltier “true” mode of the BSBW ($\theta \approx 0$ °C), see Fig. 8b: FSBW (region I), BSBW (region II), “true” mode BSBW (region III). The BSBW differs from the “true” mode BSBW, and is more diluted with the colder and fresher Barents Sea water (for more details see Dmitrenko et al., 2015). We will be interested in the transformation of the main part of the knee (region II), namely the transformation of BSBW.

In Fig. 8c the comparison of typical θ - S curves related to the St. Anna Trough (they are also shown in the other panels of Fig. 8 for reference) with that of the 92°E section of PS-96 is given: the curves 5 and 6 correspond to st. 32 and st. 42 (depth range 600–1000 m) of the PS-96 section, respectively. St. 32 was located next to the slope, while st. 42 was located about 250 km apart from the slope. The coincidence of curve 5 with a part of curve 2 implies a BSBW flow along the slope of Nansen Basin (see Fig. 4 and its legend 1). Curve 6 corresponds to the UPDW. The θ - S diagrams for CTD profiles at the section 103°E are presented by curves 8-11 (see Fig. 5 for the locations of stations). Curves 8, 9, and 10 are similar to curve 2, and indicate the BSBW. Curve 11, similar to curve 6 in Fig. 8c, corresponds to the UPDW. However, the BSBW is not observed at 126°E: see Fig. 8e, where a collection of θ - S curves (collectively referred as 12) presents all CTD profiles in the depth range 500–1800 m measured at 126°E of NABOS-09. Also we do not observe the BSBW further to the east on the 142°E section of NABOS-09 (not shown) or in the Makarov Basin.

275 The BSBW at 103°E and 126°E is also characterized by a knee-shape in σ_θ , S coordinates
(Fig. 8f, numbers correspond to those in other panels) . However the knee-shape diagram is not
observed along 126°E (curves 12) in these coordinates. The dense and cold deep waters in the
section 126°E have σ_θ , θ , S values typical for the “true” BSBW mode (Dmitrenko et al., 2015).
Nevertheless, these waters (see σ_θ , S values inside the circle; Fig. 8f) also correspond to the
280 UPDW characteristics hence cannot be distinguished as the “true” BSBW mode. To evaluate the
transformation of the “true” mode of BSBW an additional analysis is required, which is beyond
the scope of this paper.

The BSBW which is characterized by the knee-shape diagram in coordinates θ - S and σ_θ - S ,
is not visible at 126°E (Fig. 8). This is consistent with the conclusion formulated in Subsection
285 3.1.1 that by 126°E the BSBW is not accompanied by any noticeable tilt of isopycnals.
Moreover, given the characteristic feature of the θ - S structure of BSBW in the St. Anna Trough
(curves 1–4 in Fig. 8a) was observed in other years, we carried out a similar analysis using all
available CTD data and found that the BSBW is not distinct at this longitude (see Fig.9). The
only exception was 2002, when the BSBW was still observed at 126°E. It suggests that the
290 BSBW and FSBW begin to mix intensively immediately after 103°E. On the other hand, the
FSBW is well identified at 126°E and further along the slope of the Eurasian Basin (and even in
the Makarov Basin), while we cannot say the same about the BSBW. Thus, one may assume that
east of 126°E the geostrophic volume flow rate of the AW is mainly provided by the FSBW.

295

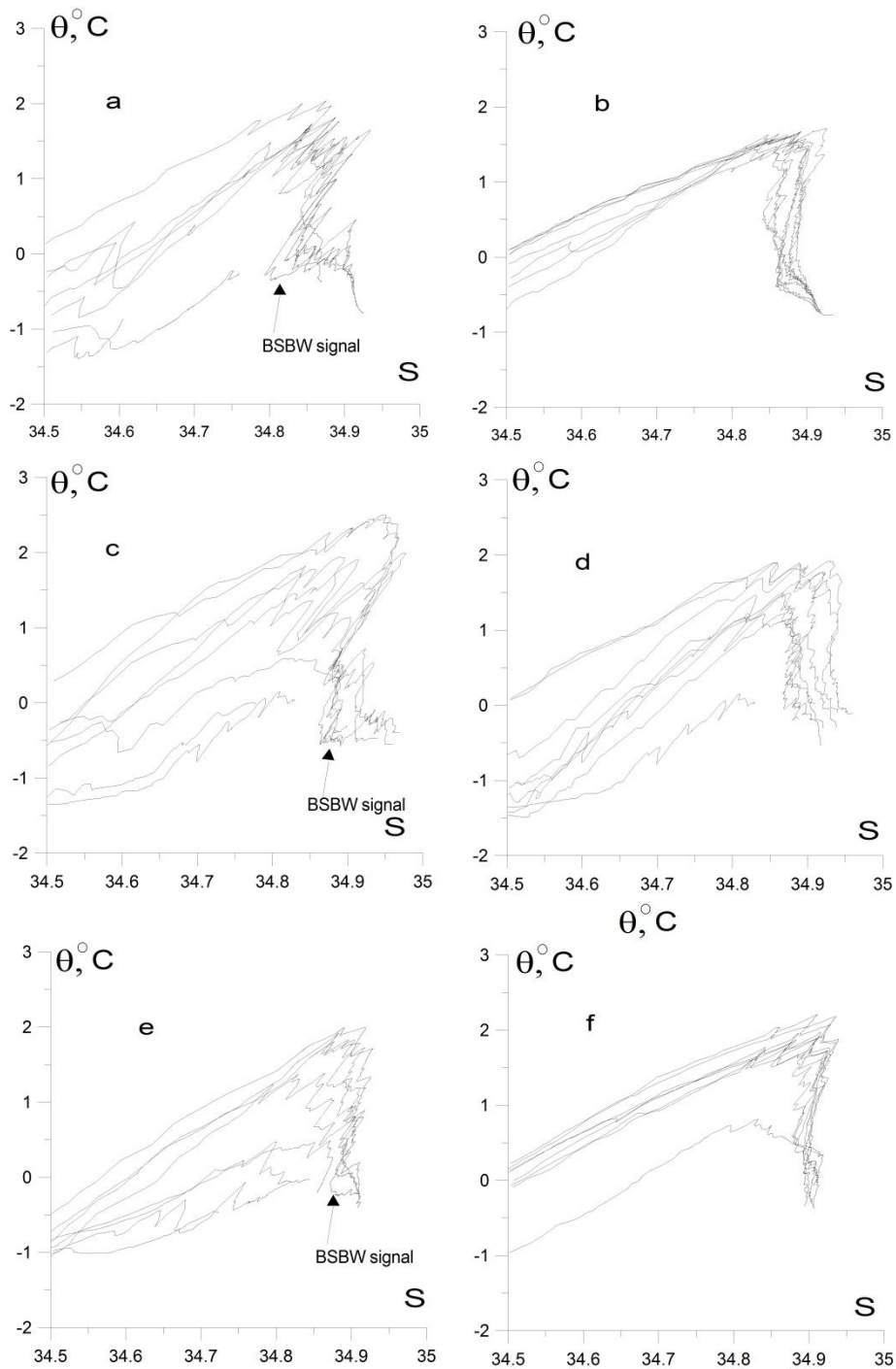


Fig. 9. θ - S diagrams based on the CTD profiling : NABOS-05: (a) and (b), 103°E (a), 126°E (b); NABOS-06: (c) and (d), 103°E (c), 126°E (d); NABOS-08: (e) and (f), 103°E (e), 126°E (f).

3.2 Characteristics of the Atlantic Water flow and geostrophic estimates of the volume flow rate

300

The estimates of the geostrophic volume flow rate and the hydrological parameters describing the AW flow in the Eurasian and Makarov Basins, are presented in Table 1. The geostrophic estimates of the near-bottom volume flow rate of the BSBW in zonal transects across the St. Anna Trough are presented in Table 2. The only exception is the transect at 82°N,

305 where the near-bottom gravity current with a considerable eastward component due to overflow
across a sufficiently deep ridge (approx. 500 m deep) east of the St. Anna Trough (Fig. 3, top
panels) makes the estimate of AW transport northward questionable. Note also that to the west
of the St. Anna Trough our estimates refer to the FSBW; to east of this region BSBW enters the
Eurasian Basin and our estimates should be attributed to the joint contribution of the two
310 branches (FSBW and BSBW).

The hydrological parameters shown in Table 1 can be interpreted as follows. The
maximum water temperature of the AW may exceed 5 °C in cases when the AW inflow to the
Eurasian Basin consists of especially warm water masses. Typical changes in the temperature
and salinity maxima of the AW moving along the slope over a distance of about 1000 km are
315 approximately 1–2 °C and 0.1, respectively. These changes lead to a slight increase in potential
density and therefore a deviation of the AW from the isopycnic distribution can be expected.
These changes are most likely associated with the exchange of heat, salt, and mass with the
surrounding waters through intrusive layering and double diffusion (see, e.g., Kuzmina et al.,
2011; Polyakov et al., 2012; Kuzmina et al., 2018) and sea ice melting and cooling (Rudels,
320 1998). The intrusions, in particular, can also contribute to the reduction of the AW heat and salt
content and the volume flow rate. The differences in the AW heat and salt content and the
volume flow rate can be clearly seen from the PS-96 section when comparing data from stations
near the continental slope of the Eurasian Basin at 92°E and from the vicinity of the Lomonosov
Ridge at 140°E.

325 It is worth noting that the maximum value of the AW temperature (θ_{max}) in this data set is
always observed in the upper layer of the Eurasian Basin at depths below the pycnocline but not
exceeding 350 m, while the maximum salinity (S_{max}) at sections in the eastern part of the Basin
can be observed at depths greater than 1000 m.

$X_{\theta_{max}}$ in Table 1 is the distance of the AW core (which can be associated with θ_{max}) from
330 the slope/shelf boundary. The highest value and the maximum variation of this parameter is
observed near 126°E and 142°E, where a two-core structure of AW is often observed
(Pnyushkov et al., 2015).

The noticeable increase of θ_{max} in 2006 at 31°E and 103°E and the intensive warming of
the AW were first reported in (Polyakov et. al., 2011). The present results show that the increase
335 of the temperature of the AW in 2006 was also accompanied by an increase of volume transport
(see Table 1, the section along 103°E and reasonings below). This can be caused not only by the
warming of the AW, but also by an increased inflow of the AW to the Eurasian Basin.

The geostrophic transport in the range of 31–159°E is characterized by a high variability (Table 1). This may be due to a) a section orientation oblique to the current; b) the difference in the horizontal scales of the sections; c) uncertainty in the choice of the reference level for geostrophic calculations; d) meandering of the flow; e) the effect of synoptic quasi-geostrophic eddies on the flow volume rate. In order to find statistically consistent estimates of the variability of geostrophic volume flow rate along the slope of the basin based on a limited data set, the following was done. The volume flow rates obtained for all sections within the range 31°–92 °E for different years were used to calculate the mean volume flow rate (region I; the number of volume flow rate values averaged is $N = 6$). Similarly, the average volume flow rate was calculated for the region 94°–107°E (region II; $N = 9$). The remaining average estimates of geostrophic volume flow rate were calculated for sections 126°E (region III; $N = 9$), 142°E (region IV; $N = 10$) and 159°E (region V; $N = 2$). Then the 95% and 80% confidence intervals were determined using the Student t-distribution. All estimates of average volume flow rates and confidence intervals are presented in Tables 1 and 2.

On the average, the volume flow rate increases from region I to region II, then decreases to region III and region IV, followed by a sharp decrease in region V. However, only the difference between the volume flow rate in region II and the values in regions IV and V are significant at 95% confidence. Transport values bounded by the confidence intervals for regions II, IV and V are (0.46; 1.72), (0.12; 0.44) and (-0.37; 0.43), respectively. These intervals indicate that the mean volume flow rate in region II exceeds the value of the same parameter in regions IV and V with a high probability of 95%. The 80% confidence intervals overlap only for regions III and IV, (0.25; 0.53) and (0.18; 0.38), respectively. In this regard, the change in the volume flow rate along the slope is significant with a probability of 80%, except for changes in volume flow rate from region III to region IV.

The above values of the mean volume flow rate and confidence intervals also suggest that the increase in volume flow rate in 2006 is significant, and not caused by the “noise” in the data. Indeed, the volume flow rates in regions II, III, and IV in 2006 exceeded the upper limits of the corresponding 95% confidence intervals. From statistical point of view such a significant increase in volume flow rates at the same time in three regions is a very rare event that can hardly be explained by random “noise” in the data caused, for example, by the influence of synoptic eddies.

Let us turn our attention to the following features of the volume flow rate estimates: high volume flow rate estimates at 96°E, 103°E, 107°E, a negative volume flow rate estimate at 126°E in 2013 and low volume flow rate estimates at 31°E, 98°E in 2009 (Table 1). Indeed, the

AW volume flow rate in the BSBW area of entry into the Eurasian Basin in 2013 was almost equal to the maximum volume flow rate in 2006 (103°E) and was quite high up to the longitude 107°E. This phenomenon as well as the intense warming in 2006 can be associated with the recent changing conditions in the Arctic. We hypothesize that the negative volume flow rate at 126°E was because of the influence of local return flows which can be observed near the slope (Pnyushkov et al., 2015). Low FSBW volume flow rate estimates in 2009 are probably associated with a strong deviation of the flow from the slope, which may underestimate the AW volume transport due to the small length of the transects to the north (see also Section 4).

The mean value of the FSBW volume flow rate in region I is $V_{mean} = 0.5$ Sv. This estimate of volume flow rate is about half the estimate of the BSBW mean volume flow rate, $V_{mean} = 0.79$ Sv ($N = 3$, Table 2). (The difference is significant at 80% confidence interval). The BSBW mean volume flow rate exceeding nearly twice the FSBW mean volume flow rate results in a dominance of the BSBW pattern of potential density contours in the longitude range of 94–107°E (region II), where both branches of the AW are present. Moreover, the sum of the mean values of the FSBW and the BSBW volume flow rate geostrophic estimates $V_{mean} = 0.5 + 0.79 = 1.29$ Sv, corresponds well with the combined FSBW and BSBW flow within the region II: $V_{mean} = 1.09$ Sv. Thus, the increase in geostrophic transport in region II is mainly due to the influence of the BSBW. The decrease in geostrophic volume flow rate in region III can also be associated primarily with the BSBW, namely, with the decrease in the BSBW transport in the 126°E section and further along the slope (see sect. 3.1.1 and 3.1.2).

Finally, at the 159°E section in the Makarov Basin, the geostrophic estimate of the along-slope volume flow rate of mixed waters of the FSBW and the BSBW has further greatly reduced down to $V_{mean} = 0.03$ Sv ($N = 2$), which is of more than one order of magnitude smaller than that in the Nansen and Amundsen Basins. Despite the low statistical significance of the latter estimate (due to small value of $N = 2$) one may conclude that the major part of the AW entering the Arctic Ocean circulates cyclonically within the Nansen and Amundsen Basins, and only its small part flows to the Makarov Basin (Rudels et al., 2015; Rudels, 2015). However, additional studies are required to confirm this result.

Table 1. Characteristics of the Atlantic Water flow in the course of its propagation along continental slope of the Eurasian Basin of the Arctic Ocean. *Dist* is the along-slope distance from the Fram Strait; θ_{max} is the maximum temperature; $\sigma_{\theta}(Z_{\theta_{max}})$, $S(Z_{\theta_{max}})$, $Z_{\theta_{max}}$, and $X_{\theta_{max}}$ are the values of potential density, salinity, depth, and lateral displacement from the slope for the point θ_{max} ; S_{max} and $Z_{S_{max}}$ are the maximum salinity and depth of S_{max} ; V is the geostrophic estimate of

405 the volume flow rate. The mean values and 95% / 80% confidence intervals of the volume rate, V_{mean} , calculated separately for CTD transects at 31–92°E, 94–107°E, 126°E, 142°E and 159°E, are also shown. The last row in the Table presents the characteristics of the return flow of the AW by the Lomonosov Rigde at the longitude 140°E and latitude 86.5°N (PS96, see Fig. 1). Year is given in the first column (e.g. NABOS06 corresponds to 2006).

<i>Exp</i>	<i>Lon</i> [°E]	<i>Dist</i> [km]	θ_{max} [°C]	$\sigma_{\theta}(Z_{\theta_{max}})$ [kg/m ³]	$S(Z_{\theta_{max}})$	$Z_{\theta_{max}}$ [m]	$X_{\theta_{max}}$ [km]	S_{max}	$Z_{S_{max}}$ [m]	V [Sv]
NABOS06	31	404	5.670	27.579	34.980	42	-11	35.099	72	0.57
NABOS08	31	404	4.883	27.771	35.103	101	0	35.105	176	0.80
NABOS09	31	404	3.691	27.818	34.999	89	0	35.002	91	0.10
NABOS09	60	856	2.503	27.891	34.951	175	10	34.981	363	0.47
NABOS13	90	1290	2.600	27.903	34.975	250	41	34.996	333	0.46
PS96	92	1322	2.786	27.875	34.960	271	33	34.968	329	0.58
$V_{mean} = 0.50 \pm 0.24 / \pm 0.14$ Sv										
NABOS15	94	1355	2.445	27.946	35.012	331	33	35.015	365	0.47
NABOS13	96	1388	2.548	27.902	34.969	207	70	34.978	264	2.06
NABOS09	98	1421	2.300	27.906	34.948	220	79	34.971	345	0.09
NABOS05	103	1561	2.029	27.870	34.876	179	39	34.934	309	0.32
NABOS06	103	1561	2.528	27.888	34.950	220	50	34.978	260	2.23
NABOS08	103	1561	1.980	27.886	34.891	201	60	34.929	325	0.42
NABOS09	103	1561	1.984	27.913	34.925	244	50	34.951	365	0.87
NABOS13	103	1561	2.278	27.904	34.942	215	80	34.956	419	1.59
NABOS13	107	1695	1.903	27.937	34.945	359	120	34.948	404	1.77
$V_{mean} = 1.09 \pm 0.63 / \pm 0.38$ Sv										
NABOS02	126	2104	1.406	27.938	34.902	324	243	34.932	2061	0.05
NABOS03	126	2102	1.341	27.941	34.899	336	342	34.921	1886	0.41
NABOS04	126	2102	1.770	27.906	34.896	271	87	34.925	2431	0.61
NABOS05	126	2102	1.695	27.936	34.926	359	227	34.935	2841	0.75
NABOS06	126	2102	1.905	27.923	34.930	284	193	34.960	968	0.77
NABOS07	126	2102	2.085	27.907	34.928	266	242	34.942	340	0.60
NABOS08	126	2102	2.195	27.885	34.911	206	235	34.939	365	0.31
NABOS09	126	2102	1.907	27.909	34.913	316	33	34.932	1018	0.40
NABOS13	126	2102	1.946	27.937	34.949	346	228	34.951	428	-0.21
NABOS15	126	2102	1.653	27.918	34.898	246	400	34.942	3816	0.22
$V_{mean} = 0.39 \pm 0.22 / \pm 0.14$ Sv										
NABOS03	142	2456	1.089	27.912	34.841	269	41	34.862	1000	0.06
NABOS04	142	2456	1.401	27.909	34.865	281	0	34.907	1608	0.21
NABOS05	142	2456	1.492	27.906	34.870	284	100	34.906	1550	0.26
NABOS06	142	2456	1.981	27.874	34.876	234	111	34.960	1016	0.60
NABOS07	142	2456	1.855	27.879	34.870	231	0	34.920	2064	0.09
NABOS08	142	2456	1.599	27.915	34.890	260	200	34.908	347	0.23
NABOS09	142	2456	1.704	27.915	34.900	253	101	34.917	1082	0.22
NABOS13	142	2456	1.475	27.940	34.909	331	115	34.926	1150	0.18
NABOS15	142	2456	1.353	27.936	34.892	326	106	34.913	1372	0.63
$V_{mean} = 0.28 \pm 0.16 / \pm 0.10$ Sv										
NABOS07	159	2783	1.424	27.887	34.839	255	0	34.880	1075	-0.01
NABOS08	159	2783	1.383	27.893	34.843	245	0	34.889	1266	0.06
$V_{mean} = 0.03 \pm 0.40 / \pm 0.10$ Sv										
PS96back	140E 86.5N	3178	1.812	27.890	34.880	219	≈ 700	34.902	472	-0.09

410

Table 2. Geostrophic estimates of the volume flow rate for near-bottom gravity flow of the Barents Sea Branch of Atlantic Water (BSBW) on zonal transects across the St. Anna Trough. The uncertainty estimates are 95% and 80% confidence intervals.

<i>Exp</i>	NABOS09	NABOS13	NABOS15	
<i>Lat</i> [°N]	81.00	81.33	81.41	V_{mean}
<i>V</i> [Sv]	0.89	0.73	0.76	$0.79 \pm 0.22 / \pm 0.10$

415

3.3 Interannual variability of the AW temperature-salinity values and the volume flow rate

Within the NABOS project, the cross-slope CTD transects at 103°E, 126°E, and 142°E were repeatedly performed for a number of annual campaigns (Table 1): 2005, 2006, 2008 and 2013 (103°E), 2002–2009, 2013 and 2015 (126°E), 2003–2009, 2013, and 2015 (142°E). We use
420 the repeated transects to describe the inter-annual variability of the AW.

Time series of the AW temperature maximum, θ_{max} , and the related values of salinity $S(\theta_{max})$ and potential density anomaly $\sigma_{\theta}(\theta_{max})$ (Fig. 10) show that the period of 2006 to 2008 was characterized by an increased temperature of the AW in the eastern part of the Eurasian Basin, an increased salinity and density reduction. The temperature excess during this period was as large
425 as 0.6–1.0 °C relative to 2002–2003 and 0.3–0.6 °C relative to 2013–2015. $S(\theta_{max})$ displayed in 2006 local maxima at the transects 126°E and 142°E, and the absolute maximum at the transect 103°E; the salinity excess for the maxima largely decreased with the longitude from approximately 0.06 at 103°E to less than 0.01 at 142°E. θ_{max} had a maximum in 2013 but only at 103°E (see Table 1 and Fig.10). The time series of $S(\theta_{max})$ display a trend of increase of AW
430 salinity over time, that can be referred to as a AW salinization in early 2000s. The salinity of AW at 142°E increases almost monotonously in the period from 2003 to 2013. The mechanism behind this salinity evolution is not clear. It is also worth noting that the maxima of θ_{max} and $S(\theta_{max})$ in 2006 and 2013 (at 103°E) were accompanied by maxima in transport.

4 Discussion

435 Here we discuss the following issues: a) differences in the identification of the BSBW; b) a comparison of the geostrophic volume flow rate estimates with other studies; c) the weakening of the BSBW signal at 126 °E and further east.

a) Advection and interaction of waters with different θ - S characteristics in the Arctic Basin, as well as the impact of climate change that has been observed over the past decade
440 (Polyakov et al., 2017) complicate an accurate identification of water masses. However, a robust approach proposed in Dmitrenko et al. (2015), is effective for distinguishing the water masses of

the FSBW and BSBW branches. As an exception, this approach fails when the FSBW temperature is below 0 °C (see Fig. 2 in Dmitrenko et al., 2015), and/or the BSBW temperature is close to 1 °C (see Fig. 6 in Schauer et al., 2002a). If such cases are rare, then either of the two approaches can be used to identify the BSBW and FSBW. Indeed, the identification of the BSBW on the PS-96 section in our case (we used the approach proposed by Dmitrenko et al., 2015; see paragraph 3.1.1) does not differ much from that proposed by Schauer et al. (2002b). However, these discrepancies can lead to almost an order of magnitude difference in estimates of the volume flow rate of the BSBW only due to the differences in the BSBW cross-sectional area.

b) Based on the velocity measurements with moored instruments (1997–2010) in the area of the West Spitsbergen Current (WSC) near Fram Strait (zonal transect at ~78°50' N), approximately 3 Sv of the AW flows into the Nansen Basin (Beszczynska-Möller et al., 2012). The long-term mean volume transport confined to the WSC core branch (or Svalbard branch in accordance with Schauer et al., 2004) included 1.3 ± 0.1 Sv of the AW warmer than 2°C. The offshore WSC branch (or Yermak branch) carried on average 1.7 ± 0.1 Sv of the AW. The variability range of the AW geostrophic transport of the Svalbard branch for meridional sections from 1997, 2001, and 2003 (summer/fall) was between 0.06 Sv and 0.7 Sv (Marnela et al., 2013). In Kolås and Fer (2018) observations of the oceanic current and thermohaline field (in summer 2015) in the three sections were used to characterize the evolution of the WSC along 170 km downstream distance. Absolute geostrophic transports of AW ranged from 0.6 Sv to 1.3 Sv in the Svalbard branch. In accordance with earlier studies of the currents in Fram Strait, recirculation of the AW can be significant, and the volume flow rate of the AW entering the Arctic Ocean ranges from 0.6 Sv to 1.5 Sv (Rudels, 1987; Aagaard and Carmack, 1989).

Our estimate of the mean volume flow rate V_{mean} in region I (31°–92 °E) is in the range of the above estimates. However, the upper confidence limit of our estimate does not reach 1 Sv. Moreover, we used $T > 0^\circ\text{C}$ to identify the AW while in Beszczynska-Möller et al. (2012) the volume flow rates of the AW entering the Eurasian Basin through Fram Strait were determined for waters with $T > 2^\circ\text{C}$. Comparatively smaller transport in region I may be because the sections along 31°E (see Fig. 1) are less than 100 km wide and do not cover the full extent of the FSBW (Fig. 2, upper panel). Given the sensitivity to the definition of AW and the resulting cross-sectional area (see point “a” above), the volume transport may be underestimated. It is possible that the formation and passage of synoptic eddies leads to variability in transport rates. According to Perez-Hernandez et al. (2017) north of Svalbard (between 21 and 33°E) in September, 2013, a large difference was found in the estimates of geostrophic volume flow rate (from 0.53 Sv to 3.39 Sv) due to the passage of eddies and meandering of the current. Våge et al.

(2016) based on geostrophic velocities at two CTD sections across the boundary current near 30° E (September, 2012) evaluated a net AW volume flow rate of 1.6 ± 0.3 Sv. They found evidence of a large eddy affecting the mean volume transport calculations. The barotropic velocity component, which is not taken into account in our estimates, can also contribute to larger transports. However, in conditions with high ice concentration in the Eurasian Basin, we might expect a reduced barotropic contribution from the sea level changes induced by wind forcing. In cruise reports, the NABOS CTD sections were characterized by ice concentrations of 50–100% (see <https://uaf-iarc.org/nabos-cruises/>). Exceptions occurred in the near-slope areas of the Laptev Sea, that is, in the sections along $\sim 126^\circ\text{E}$, where the ice concentration varied from 0 to 100%, having a maximum value in the northern part of the sections. In such areas, the contribution of the barotropic component to the flow velocity can be large. For example, using long-term measurements (1995–1996) from a mooring in the near-slope area of the Laptev Sea, Woodgate et al. (2001) showed that the contribution of the barotropic component to the velocity of the Arctic Ocean boundary current (AOBC) was equal to the contribution of the first three baroclinic modes. Assuming an average velocity based on the measurements in the upper 1200 m layer of 4.5 cm/s and a width of 50 to 84 km the volume flow rate was estimated at 5 ± 1 Sv. This is larger than our average estimate of the AW volume flow rate along 126°E (0.39 ± 0.22 , Table 1) by an order of magnitude. Such a difference can be explained not only by the absence of a barotropic contribution in our case, but also by the fact that we took into account the volume transport of AW only (i.e. the cold, low-salinity surface layer was excluded) and considered certain season (August and September). Indeed, according to long-term measurements at 6 moorings on a section along 126°E , the AOBC volume flow rate varied from 0.3 Sv to 9 Sv (Pnyushkov et al., 2018 b). Such a wide range in volume flow rate estimates is probably due to a combined effect of seasonal variability and mesoscale eddies (Pnyushkov et al., 2018 a).

The fact that seasonal variations can in some cases significantly affect the AW volume flow rates (see also the discussion in Pnyushkov et al., 2018 b) is confirmed by a number of observations (Schauer et al., 2002a; Beszczynska-Möller et al., 2012; Pnyushkov et al., 2018 b). For example, the volume flow rate of the AW in the northwestern part of the Barents Sea was 0.6 Sv (Schauer et al., 2002a). This agrees well with our estimate of the AW transport in the St. Anna Trough, 0.79 ± 0.22 Sv (Table 2). However, the analysis of current velocity measurements in the winter season at the same section in the northwestern part of the Barents Sea gave a completely different estimate of ~ 2.6 Sv (Schauer et al., 2002a).

c) According to Dmitrenko et al. (2009), the BSBW can be satisfactorily identified at 142°E . However, a “pattern” in the θ - S diagram far from the place of the BSBW entry into the Eurasian Basin can be regarded as the BSBW signal, if it maintains the similarity with the

“pattern” of the BSBW at the exit from the St. Anna Trough, that is, with the so-called “knee” (Dmitrenko et al., 2015). Our analysis showed that the “knee” is regularly observed at 103°E, while at 126°E it is absent, weak or distorted. This may be expected since the flow velocity is small, and the BSBW covers a distance from 103°E to 126°E for 1–2 years. However, despite of
515 such a long travel time, Fram Strait branch is well identified not only at 126°E, but also further along the slope. This suggests stronger transformation and mixing of, primarily, the BSBW. The BSBW transformation can be due to various reasons, including mixing with the FSBW caused by thermohaline intrusive layering at absolutely stable stratification (Merryfield, 2002; Kuzmina et al., 2014; Kuzmina, 2016), the influence of the slope topography, the impact of local
520 counterflows near the slope (see, for example, Pnyushkov et al., 2015), lateral convection (Ivanov and Shapiro, 2005; Ivanov and Golovin, 2007; Walsh et al., 2007), the impact of the Arctic Shelf Break Water (Aksenov et al., 2011; Ivanov and Aksenov, 2013) and mixing due to eddies (Schauer et al., 2002; Dmitrenko et al., 2008; Aagaard et al., 2008; Pnyushkov et al., 2018a). The understanding of the processes of transformation and mixing of the BSBW and
525 FSBW is necessary to verify an important concept proposed by Rudels, et al. (2015) that the BSBW supplies the major part of the AW to the Amundsen, Makarov and Canadian Basins, while the FSBW remains almost fully in the Nansen Basin.

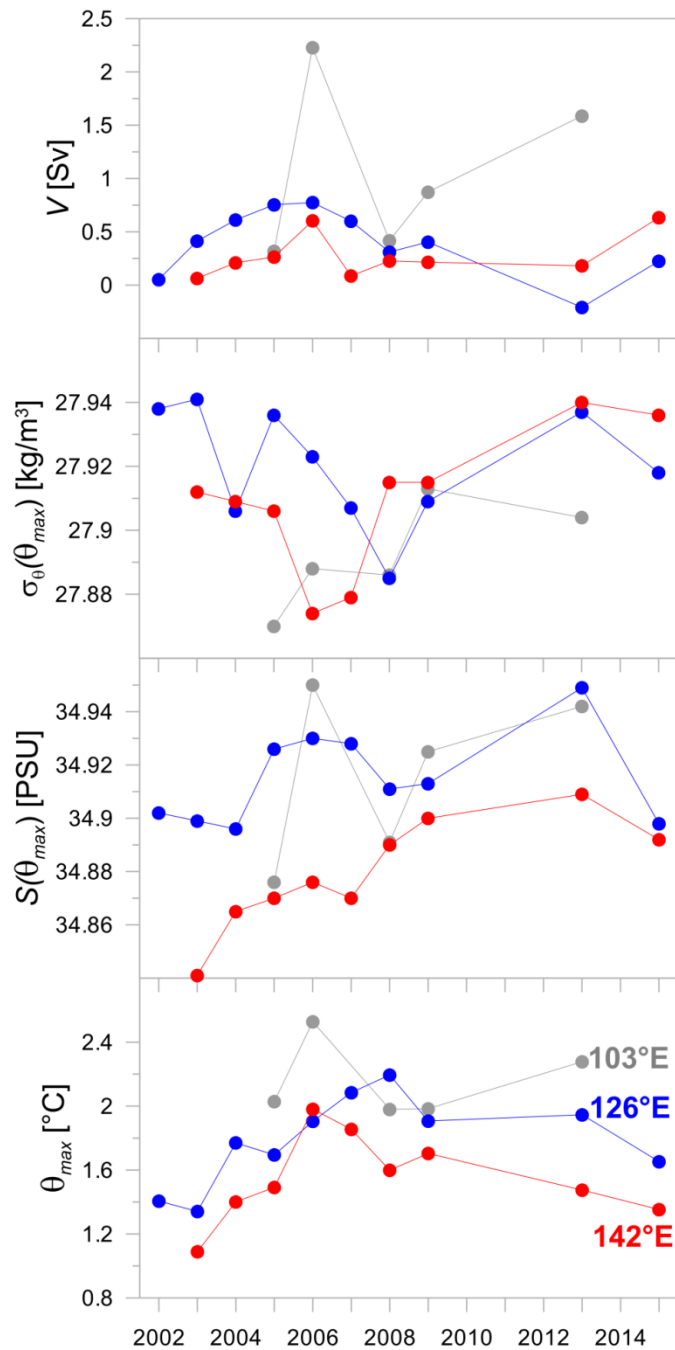
5 Summary

The θ - S properties and the volume flow rate estimates of the current carrying the AW in
530 the Eurasian Basin and St. Anna Trough were obtained based on the analysis of CTD data collected within the NABOS program in 2002–2015; additionally CTD transect PS-96 was considered.

FSBW was present at all transects, including the two transects in the Makarov Basin (159°E), while the cold waters at the transects along longitudes 126°E, 142°E and 159°E, which
535 can be associated with the influence of the BSBW, were observed in the depth range below 800 m and had little effect on the spatial structure of isopycnic surfaces and horizontal gradient of density. It is shown using θ - S analysis that the BSBW signal, which is characterized by the knee-shape feature in coordinates θ , S and σ_θ , S (see Fig.8), is either strongly weakened or not visible at the longitude 126°E (excluding the observations in 2002 at 126 °E), while the FSBW signal is
540 well identified at 126°E and further along the slope of the Eurasian Basin. Based on the revealed features of the temperature, salinity and density fields, it is suggested that east of 126°E the geostrophic volume transport of AW is mainly provided by the FSBW.

The geostrophic volume flow rate of AW increases (with 80% confidence) from the region of 31°E–92°E (0.5 ± 0.14 Sv) to the region of 94°E–107°E (1.09 ± 0.38 Sv), then decreases to the region of 126°E (0.39 ± 0.14 Sv) and becomes small (0.03 ± 0.1 Sv) in the Makarov Basin (159°E).

The temporal variability of hydrological parameters and of the AW volume flow rate is summarized as follows. The time series of θ_{max} had an absolute maximum in 2006–2008 that can be interpreted as a result of heat pulse in the early 2000s (Polyakov et al., 2011). In accordance with our analysis the time series of θ_{max} had a maximum in 2013 but only at the longitude 103°E (Table 1 and Fig.10). The time series of $S(\theta_{max})$ display a trend of increase of AW salinity over time, that can be referred to as a AW salinization in early 2000s. Moreover the salinity increases almost monotonously in the period from 2003 to 2013 at 142°E. It is important to underline also that the maxima of θ_{max} and $S(\theta_{max})$ in 2006 and 2013 (103°E) are accompanied by the volume flow rate highs. A significant increase in geostrophic volume flow rate identified in 2006 is shown to be caused by climate impact.



560 Fig. 10. Interannual variability of the maximum temperature θ_{max} and the related values of salinity $S(\theta_{max})$, potential density anomaly $\sigma_{\theta}(\theta_{max})$ and volume flow rate V on the cross-slope transects at 103°E, 126°E and 142°E.

Acknowledgments. This research, including the approach development, data processing and interpretation, performed by Nataliya Zhurbas, was funded by Russian Science Foundation, project no. 17-77-10080. Natalia Kuzmina (θ - S analysis, statistical analysis, participation in discussion) was supported by the state assignment of the Shirshov Institute of Oceanology RAS
565 (theme no. 0149-2019-0003).

The authors are very grateful to the NABOS group for providing the opportunity to use the CTD-data.

The authors are very grateful to the editor for evaluating the article and help in the work on the text and anonymous reviewers for useful comments.

570 **References**

- Aagaard, K.: On the deep circulation of the Arctic Ocean, *Deep-Sea Res.*, 28, 251–268, 1981.
- Aagaard, K., and Carmack, E. C.: The role of sea ice and other fresh water in the Arctic circulation, *J. Geophys. Res.*, 94(C10), 14485–14498, doi: 10.1029/JC094iC10p14485, 1989.
- Aagaard, K., Andersen, R., Swift, J., and Johnson, J.: A large eddy in the central Arctic Ocean, 575 *Geophys. Res. Lett.*, 35, L09601, doi: 10.1029/2008GL033461, 2008.
- Aksenov, Y., Ivanov, V. V., Nurser, A. J. G., Bacon, S., Polyakov, I. V., Coward, A. C., Naveira-Garabato, A. C., and Beszczynska-Moeller, A.: The Arctic Circumpolar Boundary Current, *J. Geophys. Res.*, 116, C09017, 1–28, doi:10.1029/2010JC006637, 2011.
- Beszczynska-Möller, A., Fahrbach, E., Schauer, U., and Hansen, E.: Variability in Atlantic water 580 temperature and transport at the entrance to the Arctic Ocean, 1997–2010, *ICES Journal of Marine Science*, 69(5), 852–863, doi: 10.1093/icesjms/fss056, 2012.
- Dmitrenko, I. A., Kirillov, S. A., Ivanov, V. I., and Woodgate, R.: Mesoscale Atlantic water eddy off the Laptev Sea continental slope carries the signature of upstream interaction, *J. Geophys. Res.*, 113, C07005, doi: 10.1029/2007JC004491, 2008.
- 585 Dmitrenko, I. A., Kirillov, S. A., Ivanov, V. V., Woodgate, R. A., Polyakov, I. V., Koldunov, N., Fortier, L., Lalande, C., Kaleschke, L., Bauch, D., Hölemann, J. A., and Timokhov, L. A.: Seasonal modification of the Arctic Ocean intermediate water layer off the eastern Laptev Sea continental shelf break, *J. Geophys. Res.-Oceans*, 114, C06010, <https://doi.org/10.1029/2008JC005229>, 2009.
- 590 Dmitrenko, I. A., Rudels, B., Kirillov, S. A., Aksenov, Y. O., Lien V. S., Ivanov, V. V., Schauer, U., Polyakov, I. V., Coward, A., and Barber, D. J.: Atlantic Water flow into the Arctic Ocean through the St. Anna Trough in the northern Kara Sea, *J. Geophys. Res.: Oceans*, 120(7), 5158–5178, doi: 10.1002/2015JC010804, 2015.
- Ivanov, V. V., and Shapiro, G. I.: Formation of dense water cascade in the marginal ice zone in 595 the Barents Sea, *Deep-Sea Res. Pt. I*, 52, 1699–1717, doi: 10.1016/j.dsr.2005.04.004, 2005.
- Ivanov, V., and Golovin, P.: Observations and modelling of dense water cascading from northwestern Laptev Sea shelf, *J. Geophys. Res.*, 112, C09003, doi:10.1029/2006JC003882, 2007.
- Ivanov, V. V., and Aksenov, E. O.: Atlantic Water transformation in the Eastern Nansen Basin: 600 observations and modelling, *Arctic and Antarctic Research*, 1(95), 72–87, 2013 (in Russian).

- Kolås, E., and Fer, I.: Hydrography, transport and mixing of the West Spitsbergen Current: the Svalbard Branch in summer 2015, *Ocean Sci.*, 14, 1603–1618, doi: 10.5194/os-14-1603-2018, 2018.
- 605 Kuzmina, N., Rudels, B., Zhurbas, V., and Stipa, T.: On the structure and dynamical features of intrusive layering in the Eurasian Basin in the Arctic Ocean, *J. Geophys. Res.*, 116, C00D11, doi: 10.1029/2010JC006920, 2011.
- Kuzmina, N. P., Zhurbas, N. V., Emelianov, M. V., and Pyzhevich, M. L.: Application of interleaving Models for the Description of intrusive Layering at the Fronts of Deep Polar Water in the Eurasian Basin (Arctic), *Oceanology*, 54(5), 557–566, doi: 610 10.1134/S0001437014050105, 2014.
- Kuzmina, N. P.: Generation of large-scale intrusions at baroclinic fronts: an analytical consideration with a reference to the Arctic Ocean, *Ocean Sci.*, 12, 1269–1277, doi: 10.5194/os-12-1269-2016, 2016.
- 615 Kuzmina, N. P., Skorokhodov, S. L., Zhurbas, N. V., and Lyzhkov, D. A.: On instability of geostrophic current with linear vertical shear at length scales of interleaving, *Izv. Atmos. Ocean. Phys.*, 54(1), 47–55, doi: 10.1134/S0001433818010097, 2018.
- Marnela, M., Rudels, B., Houssais, M.-N., Beszczynska-Möller, A., and Eriksson, P. B.: Recirculation in the Fram Strait and transports of water in and north of the Fram Strait derived from CTD data, *Ocean Sci.*, 9, 499–519, doi: 10.5194/os-9-499-2013, 2013.
- 620 Merryfield, W. J.: Intrusions in Double-Diffusively Stable Arctic Waters: Evidence for Differential mixing?, *J. Phys. Oceanogr.*, 32, 1452–1459, 2002.
- Pérez-Hernández, M. D., Pickart, R. S., Pavlov, V., Våge, K., Ingvaldsen, R., Sundfjord, A., Renner, A. H. H., Torres, D. J., and Erofeeva, S. Y.: The Atlantic Water boundary current north of Svalbard in late summer, *J. Geophys. Res.-Oceans*, 122, 2269–2290, 625 <https://doi.org/10.1002/2016JC012486>, 2017.
- Pfirman, S. L., Bauch, D., and Gammelsrød, T.: The northern Barents Sea: water mass distribution and modification, in: *The Polar Oceans and Their Role in Shaping the Global Environment*, Geophysical Monograph 85, edited by: Johannessen, O. M., Muench, R. D., and Overland, J. E., American Geophysical Union, Hoboken, NJ, 77–94, 1994.
- 630 Pnyushkov, A. V., Polyakov, I. V., Ivanov, V. V., Aksenov, Ye, Coward, A. C., Janout, M., and Rabe, B.: Structure and variability of the boundary current in the Eurasian Basin of the Arctic Ocean, *Deep-Sea Res. Pt. I*, 101, 80–97, <https://doi.org/10.1016/j.dsr.2015.03.001>, 2015.
- Pnyushkov, A. V., Polyakov, I. V., Padman, L., and Nguyen An T.: Structure and dynamics of mesoscale eddies over the Laptev Sea continental slope in the Arctic Ocean, *Ocean Sci.*, 14, 635 1329–1347, <https://doi.org/10.5194/os-14-1329-2018>, 2018a.

- Pnyushkov, A. V., Polyakov, I. V., Rember, R., Ivanov, V. V., Alkire, M. B., Ashik, I. M., Baumann, T. M., Alekseev, G. V., and Sundfjord, A.: Heat, salt, and volume transports in the eastern Eurasian Basin, *Ocean Sci.*, 14, 1349–1371, <https://doi.org/10.5194/os-14-1349-2018>, 2018b.
- 640 Polyakov, I. V., Beszczynska, A., Carmack, E. C., Dmitrenko, I. A., Fahrbach, E., Frolov, I. E., Gerdes, R., Hansen, E., Holfort, J., Ivanov, V. V., Johnson, M. A., Karcher, M., Kauker, F., Morison, J., Orvik, K. A., Schauer, U., Simmons, H. L., Skagseth, Ø., Sokolov, V. T., Steele, M., Timokhov, L. A., Walsh, D., and Walsh, J. E.: One more step toward a warmer Arctic, *Geophys. Res. Lett.*, 32, L17605, doi: 10.1029/2005GL023740, 2005.
- 645 Polyakov, I., Timokhov, L., Dmitrenko, I., Ivanov, V., Simmons, H., Beszczynska-Möller, A., Dickson, R., Fahrbach, E., Fortier, L., Gascard, J.-C., Hölemann, J., Holliday, N. P., Hansen, E., Mauritzen, C., Piechura, J., Pickart, R., Schauer, U., Walczowski, W., and Steele, M.: Observational program tracks Arctic Ocean transition to a warmer state, *Eos Trans. AGU*, 88(40), 398–399, <https://doi.org/10.1029/2007EO400002>, 2007.
- 650 Polyakov, I. V., Alexeev, V. A., Ashik, I. M., Bacon, S., Beszczynska-Möller, A., Carmack, E. C., Dmitrenko, I. A., Fortier, L., Gascard, J.-C., Hansen, E., Hölemann, J., Ivanov, V. V., Kikuchi, T., Kirillov, S., Lenn, Y.-D., McLaughlin, F. A., Piechura, J., Repina, I., Timokhov, L. A., Walczowski, W., and Woodgate, R.: Fate of Early 2000s Arctic Warm Water Pulse, *Bulletin of the American Meteorological Society*, 92(5), 561–566, doi: 10.1175/2010BAMS2921.1, 2011.
- 655 Polyakov, I. V., Pnyushkov, A., Rember, R., Ivanov, V., Lenn, Y.-D., Padman, L., and Carmack, E. C.: Mooring-based observations of the double-diffusive staircases over the Laptev Sea, *J. Phys. Oceanogr.*, 42, 95–109, doi: 10.1175/2011JPO4606.1, 2012.
- Polyakov, I. V., Pnyushkov, A. V., Alkire, M. B., Ashik, I. M., Baumann, T. M., Carmack, E. C., 660 Goszczko, I., Guthrie, J., Ivanov, V. V., Kanzow, T., Krishfield, R., Kwok, R., Sundfjord, A., Morison, J., Rember, R., and Yulin, A.: Greater role for Atlantic inflows on sea-ice loss in the Eurasian Basin of the Arctic Ocean, *Science*, 356, 285–291, <https://doi.org/10.1126/science.aai8204>, 2017.
- Rudels, B.: On the mass balance of the polar ocean, with special emphasis on the Fram Strait, 665 *Skr. Nor. Polarinst.*, 188, 1–53, 1987.
- Rudels, B., Jones, E. P., Anderson, L. G., and Kattner, G.: On the intermediate depth waters of the Arctic Ocean, in: *The Role of the Polar Oceans in Shaping the Global Climate*, edited by: Johannessen, O. M., Muench, R. D., and Overland, J. E., American Geophysical Union, Washington, DC, 33–46, 1994.

- 670 Rudels, B.: Aspects of Arctic oceanography, in *Physics of ice-covered seas*, vol. 2, edited by: Leppäranta, M., Univ. Press, Helsinki, 517–568, 1998.
- Rudels, B., Björk, G., Muench, R. D, and Schauer, U.: Double-diffusive layering in the Eurasian Basin of the Arctic Ocean, *J. Mar. Syst.*, 21(1–4), 3–27, doi: 10.1016/S0924-7963(99)00003-2, 1999.
- 675 Rudels, B., Jones, E. P., Schauer, U., and Eriksson, P.: Atlantic sources of the Arctic Ocean surface and halocline water, *Polar research*, 23(2), 181–208, doi: 10.1111/j.1751-8369.2004.tb00007.x, 2006.
- Rudels, B.: Arctic Ocean circulation, processes and water masses: A description of observations and ideas with focus on the period prior to the International Polar Year 2007–2009, *Progress in Oceanography*, 132, 22–67, doi: 10.1016/j.pocean.2013.11.006, 2015.
- 680 Rudels, B., Korhonen, M., Schauer, U., Pisarev, S., Rabe, B., and Wisotzki A.: Circulation and transformation of Atlantic water in the Eurasian Basin and the contribution of the Fram Strait inflow branch to the Arctic Ocean heat budget, *Progress in Oceanography*, 132, 128–152, doi: 10.1016/j.pocean.2014.04.003, 2015.
- 685 Schauer, U., Muench, R. D., Rudels, B., and Timokhov, L.: Impact of eastern Arctic shelf waters on the Nansen Basin intermediate layers, *J. Geophysical Res.*, 102(C2), 3371–3382, 1997.
- Schauer, U., Loeng, H., Rudels, B., Ozhigin, V. K., and Dieck, W.: Atlantic Water flow through the Barents and Kara Seas, *Deep-Sea Res. Pt. I*, 49(12), 2281–2298, [https://doi.org/10.1016/S0967-0637\(02\)00125-5](https://doi.org/10.1016/S0967-0637(02)00125-5), 2002a.
- 690 Schauer, U., Rudels, B., Jones, E. P., Anderson, L. G., Muench, R. D., Björk, G., Swift, J. H., Ivanov, V., and Larsson, A.-M.: Confluence and redistribution of Atlantic water in the Nansen, Amundsen and Makarov basins, *Ann. Geophys.*, 20, 257–273, doi: 10.5194/angeo-20-257-2002, 2002b.
- Schauer, U., Fahrbach, E., Osterhus, S., and Rohardt, G.: Arctic warming through the Fram Strait: Oceanic heat transport from 3 years of measurements, *J. Geophysical Res.*, 109(C06026), doi: 10.1029/2003JC001823, 2004.
- 695 Swift, J. H., Jones, E. P., Aagaard, K., Carmack, E. C., Hingston, M., MacDonald, R. W., McLaughlin, F. A., Perkin, R. G.: Waters of the Makarov and Canada basins, *Deep-Sea Res. II*, 44(8), 1503–1529, doi: 10.1016/S0967-0645(97)00055-6, 1997.
- 700 Våge, K., Pickart, R. S., Pavlov, V., Lin, P., Torres, D. J., Ingvaldsen, R., Sundfjord, A., and Proshutinsky, A.: The Atlantic Water boundary current in the Nansen Basin: Transport and mechanisms of lateral exchange, *J. Geophys. Res.*, 121, 6946–6960, <https://doi.org/10.1002/2016JC011715>, 2016.

Walsh D., Polyakov I., Timokhov L., and Carmack E.: Thermohaline structure and variability in
705 the eastern Nansen Basin as seen from historical data, *Journal of Marine Research*, 65, 685–
714, 2007.

Woodgate, R. A, Aagaard, K., Muench, R. D., Gunn, J., Bjork, G., B. Rudels, Roach, A. T., and
Schauer, U.: The Arctic Ocean boundary current along the Eurasian slope and the adjacent
710 Lomonosov Ridge: Water mass properties, transports and transformations from moored
instruments, *Deep-Sea Res. Pt. I*, 48(8), 1757–1792, [https://doi.org/10.1016/S0967-
0637\(00\)00091-1](https://doi.org/10.1016/S0967-0637(00)00091-1), 2001.

Zhurbas, N. V.: Estimates of transport and thermohaline characteristics of the Atlantic Water in
the Eurasian Basin, *Russian Meteorology and Hydrology*, 44, 603–612,
doi: 10.3103/S1068373919090048, 2019

715

Variability of the thermohaline structure and transport of Atlantic water in the Arctic Ocean based on NABOS CTD hydrography data

Nataliya Zhurbas¹ and Natalia Kuzmina¹

5 ¹Shirshov Institute of Oceanology, Russian Academy of Sciences, 36 Nakhimovsky Prospekt ,
117997 Moscow, Russia

Correspondence to: Nataliya Zhurbas (nvzhurbas@gmail.com)

Abstract. CTD Conductivity-temperature-depth (CTD) transects across continental slope of the Eurasian Basin and the St. Anna Trough performed during NABOS (Nansen and Amundsen
10 Basins Observing System) project in 2002–2015 and a transect from the Polarstern-1996 expedition are used to describe θ - S the temperature and salinity characteristics and volume flow rates of the current carrying the Atlantic Water (AW) in the Arctic Ocean. The CTD dataset includes 33 sections in the Eurasian Basin, 4 transects in the St. Anna Trough and 2 transects in the Makarov Basin; additionally a CTD transect of the Polarstern 1996 expedition (PS 96) is
15 used. The variability of thermohaline pattern on the AW on its pathway along the slope of Eurasian Basin is investigated. The A dynamic Fram Strait branch of the Atlantic Water (FSBW) is identified on all transects, including two transects in the Makarov Basin (along 159°E), while the cold waters on the eastern transects along 126°E, 142°E and 159°E, which can be associated with the influence of the Barents Sea branch of the Atlantic water (BSBW), on the transects
20 along 126°E, 142°E and 159°E, were observed in the depth range below 800 m and had a negligible effect on the spatial structure of isopycnic surfaces. An interpretation of the spatial and temporal variability of hydrological parameters characterizing the flow of the AW in the Eurasian Basin is presented. The geostrophic volume transport of AW decreases farther away from the areas of the AW inflow to the Eurasian Basin, decreasing by one order of magnitude in
25 the Makarov Basin at 159°E, implying that the major part of the AW entering the Arctic Ocean circulates cyclonically within the Nansen and Amundsen Basins. There is an absolute maximum of θ_{max} (AW core temperature) in 2006–2008 time series and a maximum in 2013, but only at 103°E. Salinity $S(\theta_{max})$ (AW core salinity) time series display an increase of the AW salinity in 2006–2008 and 2013 (at 103°E) that can be referred to as a AW salinization in the early 2000s.
30 The maxima of θ_{max} and $S(\theta_{max})$ in 2006 and 2013 are accompanied by the volume transport maxima. The time average geostrophic volume transports of AW, V_{mean} , are $V_{mean} = 0.5 \text{ Sv}$ are 0.5 Sv in the longitude range 31–92°E, $V_{mean} = 0.8 \text{ Sv}$ 0.8 Sv in the St. Anna Trough and $V_{mean} = 1.1 \text{ Sv}$ 1.1 Sv in the longitude range 94–107°E.

1 Introduction

35 Atlantic water (AW) enters the Eurasian Basin by ~~in~~ two branches (see, e.g., Aagaard, 1981; Rudels et al., 1994; Schauer et al., 1997; Rudels et al., 1999; Schauer et al., 2002a, b; Rudels et al., 2006; Berzczynska-Möller et al., 2012; Rudels et al., 2015; Rudels, 2015; Dmitrenko et al., 2015; Pnyushkov et al., 2015, 2018b): one ~~of them~~ ~~branch~~ originates from the Greenland and Norwegian seas and flows to the basin through ~~the~~ Fram Strait (~~the~~ Fram Strait
40 branch of the Atlantic Water, hereinafter the FSBW), and the other reaches the deep part of the Arctic Ocean near St. Anna Trough after passing through the Barents Sea (~~the~~ Barents Sea branch of the Atlantic water, hereinafter the BSBW). After entering the Eurasian Basin the FSBW moves eastward with ~~the~~ ~~a~~ subsurface boundary current and has a core of higher temperature and salinity ~~than the BSBW~~. In the longitude range of 80–90°E, it encounters and
45 partially mixes with the BSBW, which is strongly cooled due to mixing with shallow waters of the Arctic shelf seas and atmospheric impact (Schauer et al., 1997; 2002a, b). Further, the water masses resulting from the interaction of ~~the~~ two branches ~~which transport the AW continue spreading cyclonically in the Eurasian Basin.~~

To study the characteristics of the ~~FSBW and BSBW flow in the Eurasian Basin, it is useful to estimate, first of all, its volume flow rate in different parts of the basin. Generally the estimates of the AW volume flow rate have been based on direct current observations (Fahrbaach et al., 2001; Berzczynska Möller et al., 2012; Rudels et al., 2014; Pnyushkov et al., 2015). However, it is useful also to consider the AW geostrophic volume flow rate calculated on the basis of CTD data. Such estimates, obtained for different regions of the Arctic Ocean, were given in a number~~
55 ~~of papers (e.g. Marnela et al., 2013; Våge et al., 2016; Pérez-Hernández et al., 2017; Kolås and Fer, 2018). For completeness, it is of interest to carry out estimates of the AW geostrophic volume flow rate along continental slope of the Eurasian Basin based on a large volume of empirical data.~~

Within the NABOS (Nansen and Amundsen Basins Observing System) project (Polyakov
60 et al., 2007) a unique volume of CTD data was collected: more than 30 sections were made in various regions of the Arctic Basin in the summer/fall 2002-2015. A number of sections in different years were made in the same regions of the Basin, which allows studying the interannual variability of the water masses thermohaline structure and the geostrophic volume flow rate in these areas.

65 The main goal of this work is to investigate the spatial and temporal variability of the AW geostrophic volume flow rate during its propagation along the continental slope of the Eurasian Basin. ~~Another important aspect of our analysis is the investigation of~~ ~~We further discuss~~ the

thermohaline structure and transformation of the FSBW and BSBW. ~~Such analysis is essential for two reasons: a) The estimates of the AW transport are sensitive to the temperature and salinity ranges used for the identification of this water (Pnyushkov et al., 2018b); b) it is reasonable to assume that~~, and mixing of FSBW, BSBW and surrounding waters may change the AW geostrophic volume flow rate.

2 Material and Methods

We used data ~~of~~ from the CTD ~~profiling on~~ transects across the slope of the Eurasian Basin in the longitude range of 31–159°E measured in the years 2002–2015 within the framework of NABOS project (in total 39 transects). The data are freely available at the site <http://nabos.iarc.uaf.edu>. In addition, a CTD transect across the entire Eurasian Basin and over the Lomonosov Ridge starting at 92°E at the slope from R/V *Polarstern* in 1996 (hereafter PS96) was also included. The locations of the CTD transects are shown in Fig. 1. ~~It can be seen from the map in Fig. 1 that m~~ Most of the CTD transects are aligned cross-slope and grouped at longitudes of 31, 60, 90, 92, 94, 96, 98, 103, 126, 142, and 159°E. Four of the 40 transects crossed zonally the St. Anna Trough (at the latitude of 81, 81.33, 81.42, and 82°N) through which the BSBW enters the Eurasian Basin. Most of the CTD casts covered the upper layer from the sea surface to either 1000 m depth or to the bottom (if the total depth of the sea was shallower less than 1000 m); some of the CTD casts (a. Approximately every third or fourth) covered the depths from the sea surface cast was down to the sea bottom even if the sea depth exceeded 1000 m.

To estimate the ~~strength of the FSBW or the BSBW or both branches~~ volume transport of the Atlantic Water, we applied standard dynamical method. The no-motion level (the depth of zero velocity ~~depth~~) was determined from the following consideration. If the baroclinic current occupies the upper layer or/and some intermediate layer, the no-motion level can be chosen in a calm deep layer (where the horizontal density gradient is relatively small). On the contrary, in case of a near-bottom gravity flow, the no motion level can be reasonably chosen somewhere well above the near-bottom flow. We adopted for the level of no-motion level either 1000 m depth or the sea bottom depth if the latter was smaller than 1000 m for the FSBW, and some level in the vicinity of approximately 50 m depth, where density contours were more or less flat, for the observations of BSBW in the St. Anna Trough (see also below).

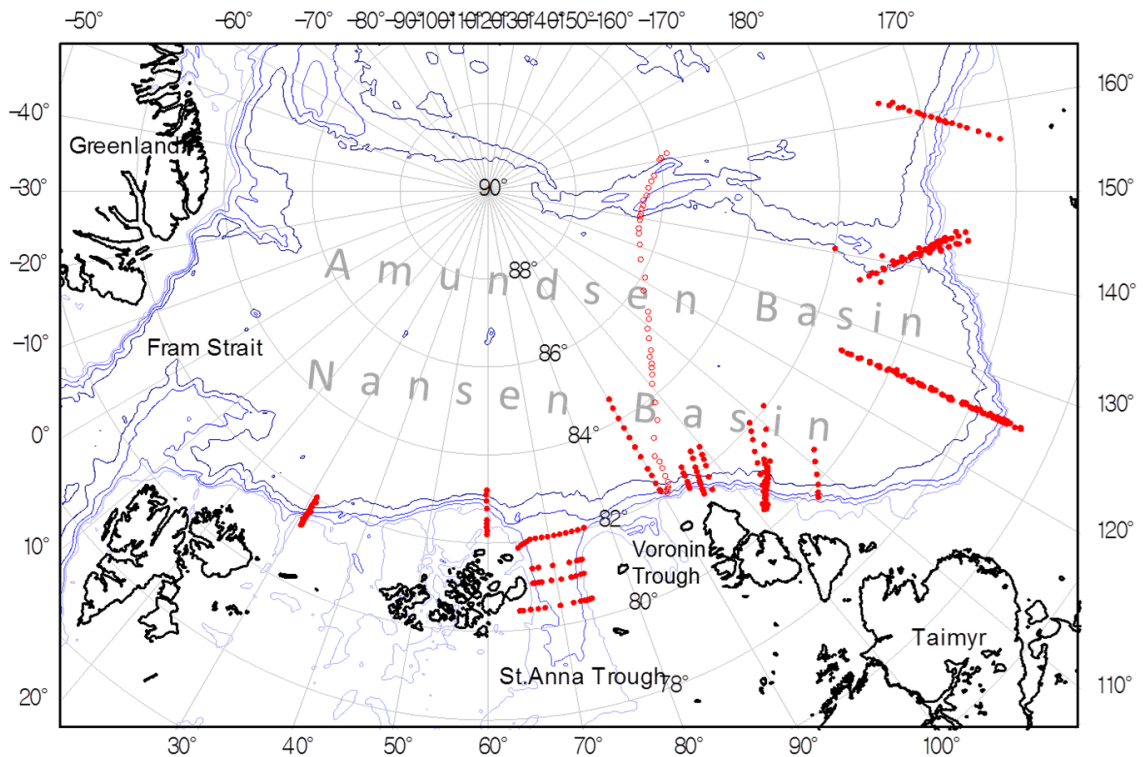


Fig. 1. Bathymetric map of the Eurasian Basin with 300, 500, 1000, and 2000 m contours shown. The red filled and blank circles are the locations of CTD stations on the NABOS and PS96 transects, respectively.

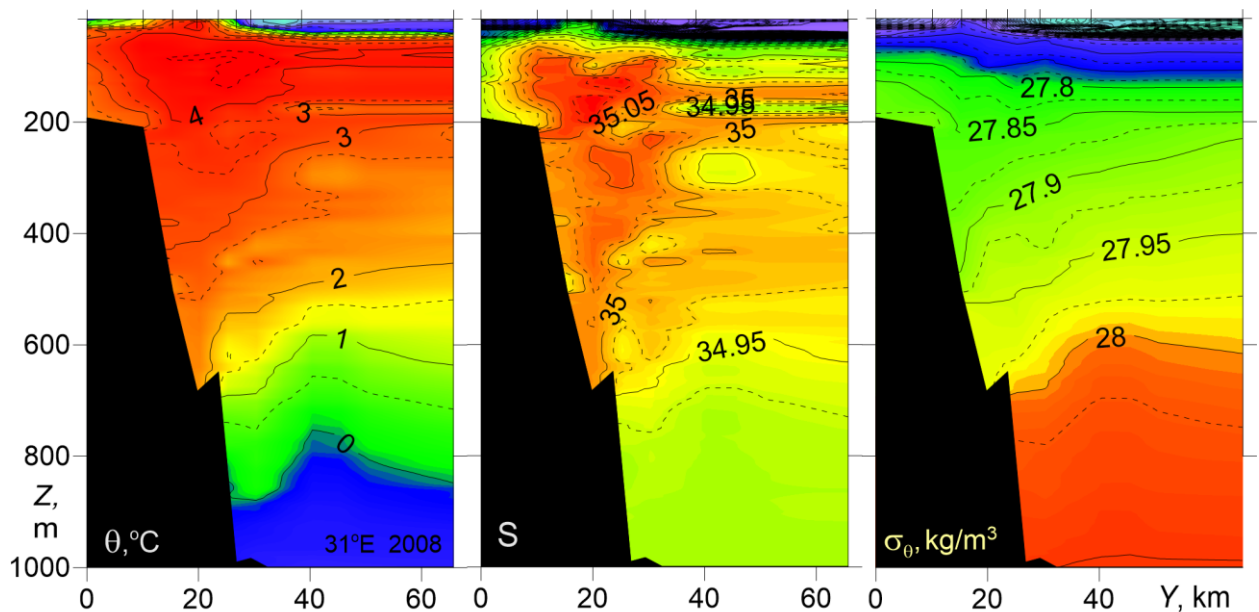
Since the FSBW brings saline and warm water to the Eurasian Basin, the geostrophic estimates of the volume flow rate were **transport was** found by integration over the depth range with positive temperature, $\theta > 0$ °C, and relatively high salinity, $S > 34.5$ (the salinity is given in the practical salinity scale), that is, **some areas in the near-surface layers** with warm and fresh water (which cannot be attributed to AW) were excluded. For the observations of BSBW in the St. Anna Trough the geostrophic estimates of the volume flow rate were found **transport was calculated** by integration over a depth range with the **non-averaged** temperature below 0 °C and the salinity above 34.5. If both AW branches of AW were present on the transect, the integration was performed over the entire depth range **except but excluding** the cold near-surface layer ($\theta < 0$ °C) and the **areas in the near-surface layer** with warm ($\theta > 0$ °C) and relatively fresh ($S < 34.5$) water **near-surface layer**. The zero velocity depth in this case was chosen **in accordance to after inspection of** the observed pattern of density contours, i.e. **its resemblance with suggesting** either the near-surface flow pattern or the near-bottom flow pattern (see Section 3). The details and limitation of the geostrophic velocity calculations are discussed in Zhurbas (2019).

3. Results

3.1 Variability of the thermohaline pattern on the AW pathway along the slope of Eurasian Basin

3.1.1 CTD transects analysis

120 The transformation of thermohaline signatures (i.e. patterns of salinity S , potential
 temperature θ , and potential density anomaly σ_θ , versus cross-slope distance and depth) of the
 AW flow on its pathway along the slope of the Eurasian Basin are presented in Fig.2. The σ_θ
 contours on transects at 31°E diverge towards the continental slope margin (to the south),
 shallowing above the warm/saline core of the AW and sloping down beneath it associated with a
 125 eastward subsurface flow. Such a structural feature of the distribution of isopycnic surfaces was
 observed on all NABOS transects taken across available continental slope at 31°E. According to
 Fig. 2 the warm/saline core of the Fram Strait Branch of the AW with the maximum temperature
 θ_{max} of 4.88°C at the depth $Z_{\theta_{max}}=102$ m and the maximum salinity S_{max} of 35.11 at the depth
 $Z_{S_{max}}=176$ m is found on the slope at about 1000 m isobath.

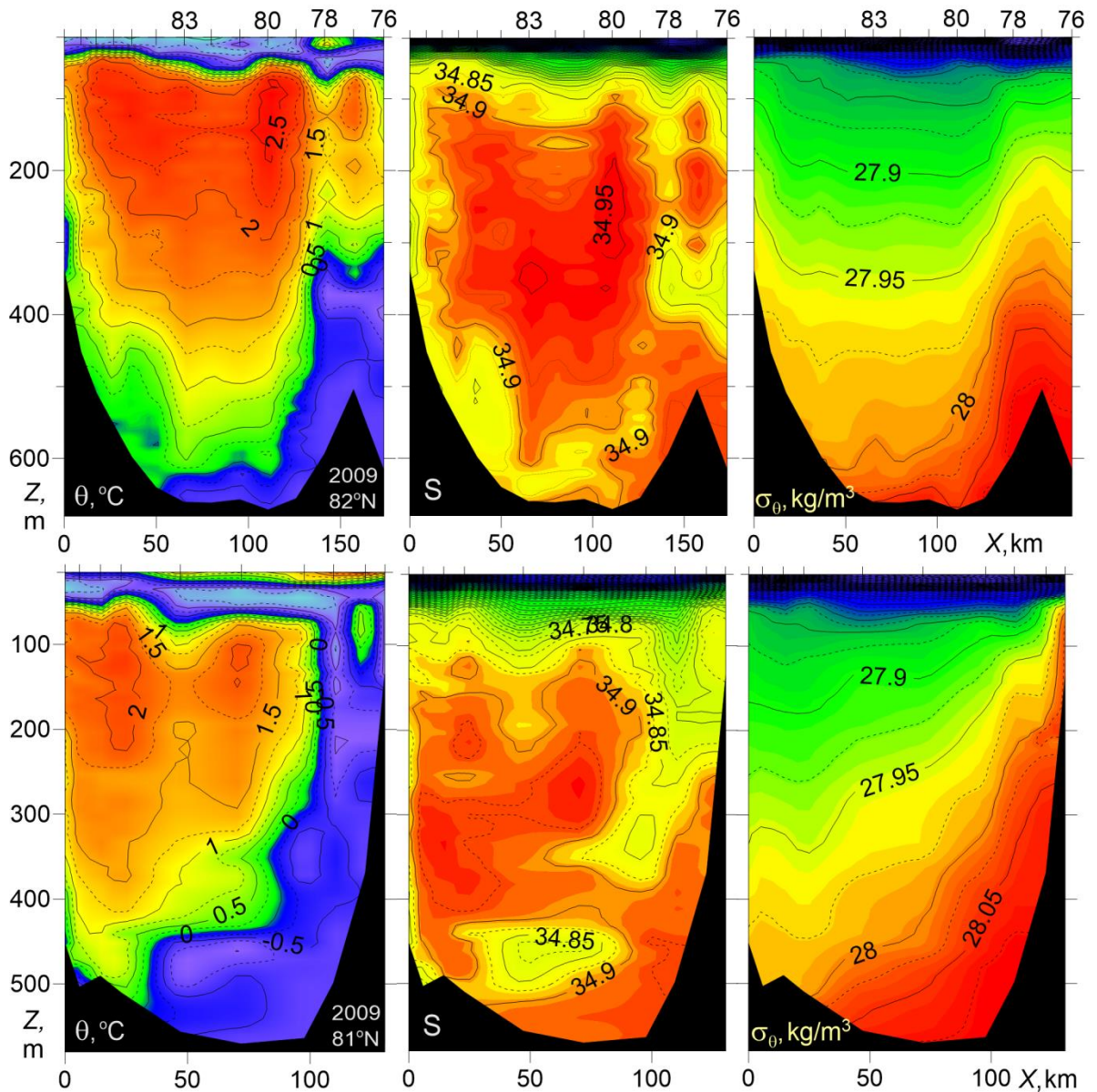


130

Fig. 2. Temperature θ , salinity S , and potential density anomaly σ_θ versus cross-slope distance and depth for the NABOS-2008 transect across the Eurasian Basin slope at 31°E.

Figure 3 presents temperature, salinity, and potential density versus distance and depth for two zonal transects across the St. Anna Trough at latitudes of 81 and 82°N. A stable pool of cold
 135 ($\theta < 0^\circ\text{C}$) and dense ($\sigma_\theta > 28 \text{ kg/m}^3$) water in the bottom layer is seen adjacent to the eastern slope of the trough. The transfer of the densest water pool to the eastern slope corresponds to a geostrophically balanced near-bottom gravity flow to the North. Note, that the gravity bottom currents are a typical feature of ocean dynamics and can develop in the narrows and troughs of various ocean basins (Arneborg et al., 2007; Zhurbas et al., 2012). This near-bottom gravity

140 current carries also waters of Atlantic origin, which are strongly cooled due to mixing with
 shallow waters of the Arctic shelf seas shelf waters in (the Barents and Kara seas). Above the
 near-bottom gravity flow of the BSBW one can observe two-core structure of warm FSBW with
 temperature up to 2.5 °C that enters the St. Anna Trough from the north-west at the western side
 of the trough and leaves it for the north-east at the eastern side of the trough. At 82°N, the
 145 BSBW overflows a ridge-like elevation east of the St. Anna Trough (top panels in Fig. 3).
 Results of s Studies of the currents velocities and thermohaline characteristics of the waters
 masses and hydrography in the St. Anna Trough can be found in (Schauer et al., 2002a, b;
 Rudels et al., 2014 2015; Dmitrenko et al., 2015).



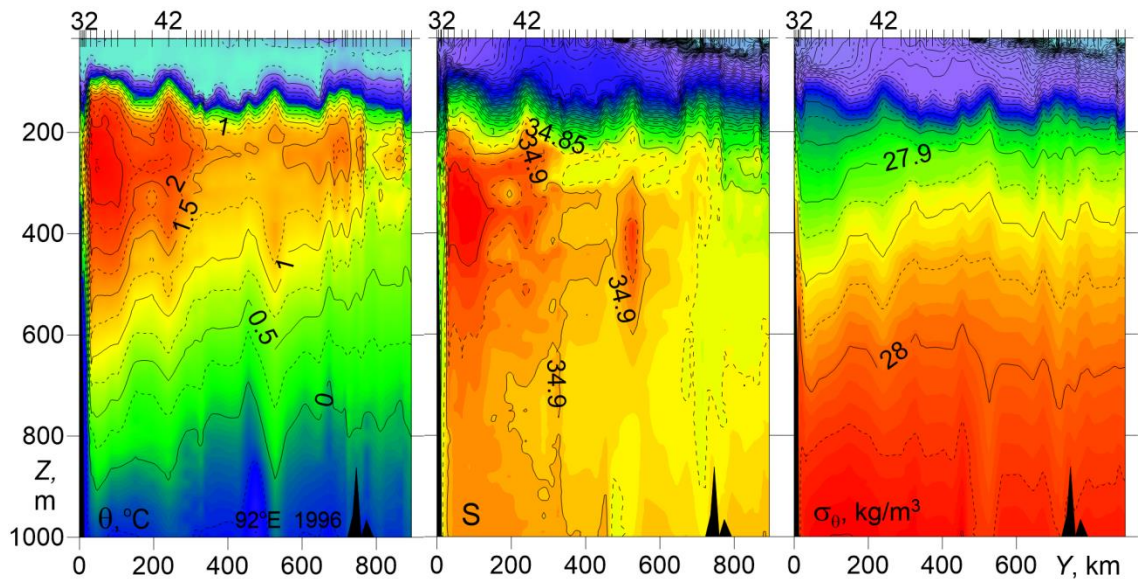
150 Fig. 3. Temperature θ , salinity S , and potential density anomaly σ_θ versus distance and depth for
 zonal transects across the St. Anna Trough at latitudes of 81°N (bottom, NABOS-2009), and
 82°N (top, NABOS-2009). The X-axis is directed to the east.

In order to understand the effect of the FSBW and the BSBW transformation on geostrophic volume flow rate, it is necessary to identify water masses of different origin. For that purpose the following criterion is often used (Walsh et al., 2007; Pfirman et al., 1994): the water masses of the FSBW are characterized by $\theta > 0$ °C, and the BSBW can be identified by the following expressions: -2 °C $< \theta < 0$ °C, $34.75 < S < 34.95$ and $27.8 \text{ kg/m}^3 < \sigma_\theta < 28.0 \text{ kg/m}^3$. Other approaches to define BSBW are given in Schauer et al. (1997; 2002a, b) and Dmitrenko et al. (2015). According to Schauer et al. (1997; 2002a, b) the BSBW includes all waters that enter the Nansen Basin from the St. Anna and Voronin troughs. The temperature of these waters, however, can reach ~ 1 °C. The justification for this approach was based on θ - S analysis of the waters of the north-eastern part of the Barents Sea and the St. Anna and Voronin troughs. According to Dmitrenko et al. (2015), the BSBW consists of two water masses, and the temperature of the warmer water mass can only slightly exceed 0 °C (for more details see section 3.1.2). Here we will rely on the definitions of the FSBW and BSBW proposed by Dmitrenko et al. (2015).

In Fig. 4 the CTD transect at 92°E carried out in the *Polarstern*-1996 expedition just east of the entrance point of the BSBW to the Eurasian Basin from the St. Anna Trough and Voronin Trough is presented. It can be assumed that a part of the BSBW extends deep into the Basin, mixing with the FSBW, while another part of the BSBW moves flows eastward along the slope according to the general cyclonic circulation observed in the Eurasian Basin. On the presented transect the BSBW is observed in the depth range below 600 m as a narrow, about 10 km wide strip of cold water near the slope (see also Subsection 3.1.2) adjacent to a 300 km wide zone occupied by the warm FSBW. The pattern of the potential density distribution of FSBW on this transect is similar to transects at 31°E. Namely, despite of the masking effect of vertical undulations of σ_θ contours caused by internal waves and mesoscale eddies (one of subsurface, intra-pycnocline eddies is probably identified at the distance of $Y=510$ km), one cannot miss the tendency of shallowing/sloping down the σ_θ contours isopycnals tend to shoal/deepen above/below the FSBW core towards the continental slope margin (to the south) which, in terms of geostrophic balance implies the eastward flow of FSBW. The FSBW core on the 92°E transect is found at 40 km distance from the slope, with the maximum temperature $\theta_{max}=2.79$ °C at $Z_{\theta_{max}}=271$ m and salinity $S_{max}=34.97$ at $Z_{S_{max}}=329$ m. Therefore, the FSBW on its pathway along the slope of the Eurasian Basin from 31°E to 92°E has cooled, desalinated, sank and become denser by approx. about 2 °C, 0.1, 150 m, and 0.1 kg/m³, respectively. Another significant distinct feature seen in the PS96 transect is an a layer with increased temperature pool

in the layer of between 180 and 300 m at the distance of depth at $Y=600-750$ km in the vicinity of the Lomonosov Ridge, which can be attributed to the geostrophically-balanced FSBW return flow cyclonically circulating around the Eurasian Basin (Rudels et al., 1994; Swift et al., 1997).

190 According to Schauer et al. (2002b) ~~where the thermohaline structure along~~ who studied the PS-96 section ~~was studied in detail~~, the horizontal and vertical scales of the BSBW were taken at 30 km and 800 m, respectively. This differs from our interpretation based on the definition of BSBW with temperature less than 0°C .



195 Fig. 4. Temperature θ , salinity S , and potential density anomaly σ_θ versus distance and depth for cross-shelf transects at 92°E (PS-1996).

Further east, in the longitude range of $94-107^\circ\text{E}$ (NABOS-09), the denser part of BSBW ~~dives~~ under the FSBW; ~~is~~ characterized by an eastward geostrophic current with isopycnals sloping towards the North in a 150 km wide zone adjacent to the slope (see Fig. 5, top panel).

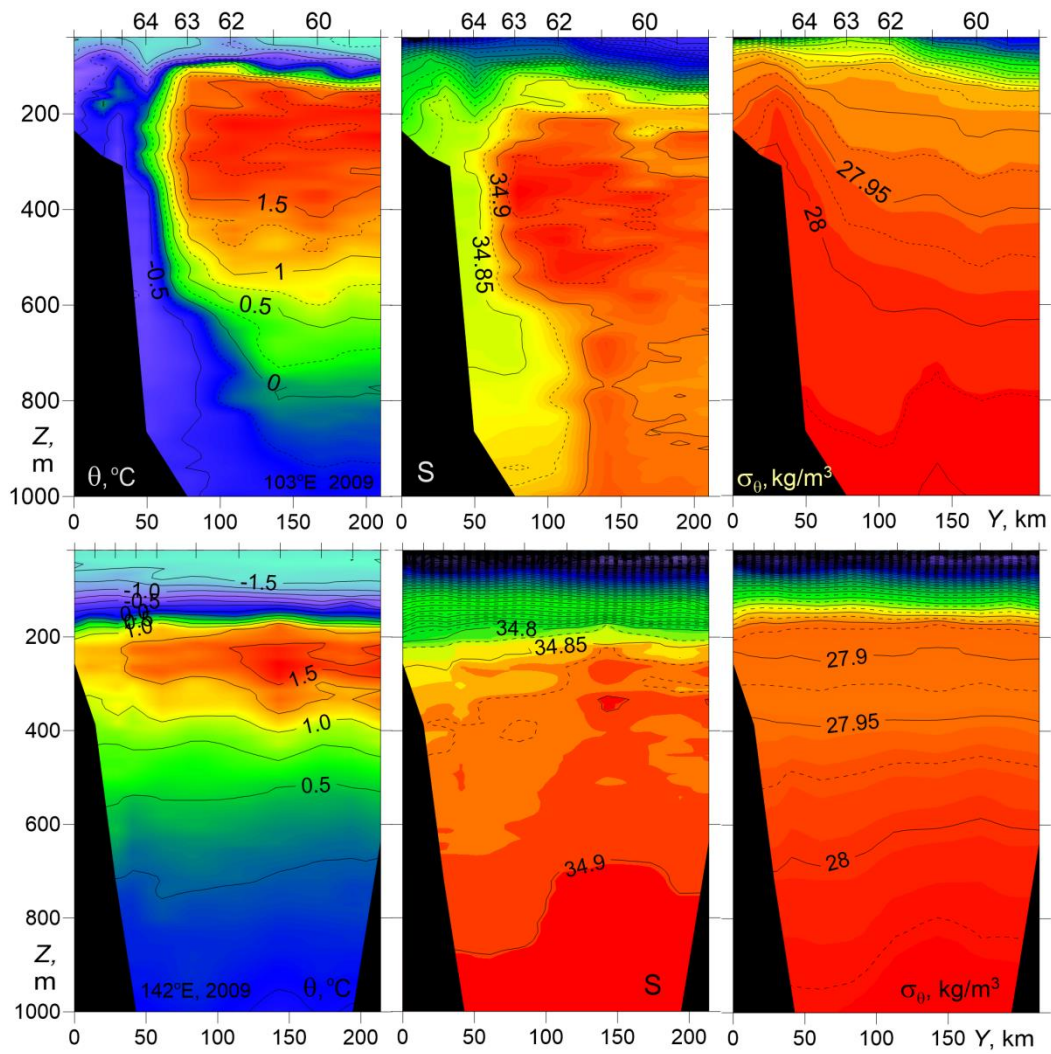
200 Less saline water at the slope is the less dense ~~Barents Sea Branch water~~ BSBW that has entered the Nansen Basin when the slope narrows north of Severnaya Zemlya (Schauer et al., 1997).

The vertical location of the FSBW layer ~~has not changed much relative~~ is similar to the 92°E in the section PS-96 but the maximum temperature has further decreased: in the transect in Fig. 5, the top panel, $\theta_{max}=1.98^\circ\text{C}$ at $Z_{\theta_{max}}=245$ m and $S_{max}=34.95$ at $Z_{S_{max}}=365$ m. The bottom panel of Fig. 5 presents the ~~data from~~ transect at 142°E (NABOS-09) which is located on the Lomonosov Ridge, between the Amundsen and Makarov Basins. The comparison of the two transects obtained in the same year shows that the vertical scale of the especially warm FSBW water ($\theta > 1.5^\circ\text{C}$) has significantly decreased. Nevertheless, the FSBW waters are also observed at this longitude and affect the slopes of isopycnic surfaces in a layer up to 300 m. The cold waters with $\theta < 0^\circ\text{C}$, which can be associated with the BSBW, are observed only at two stations

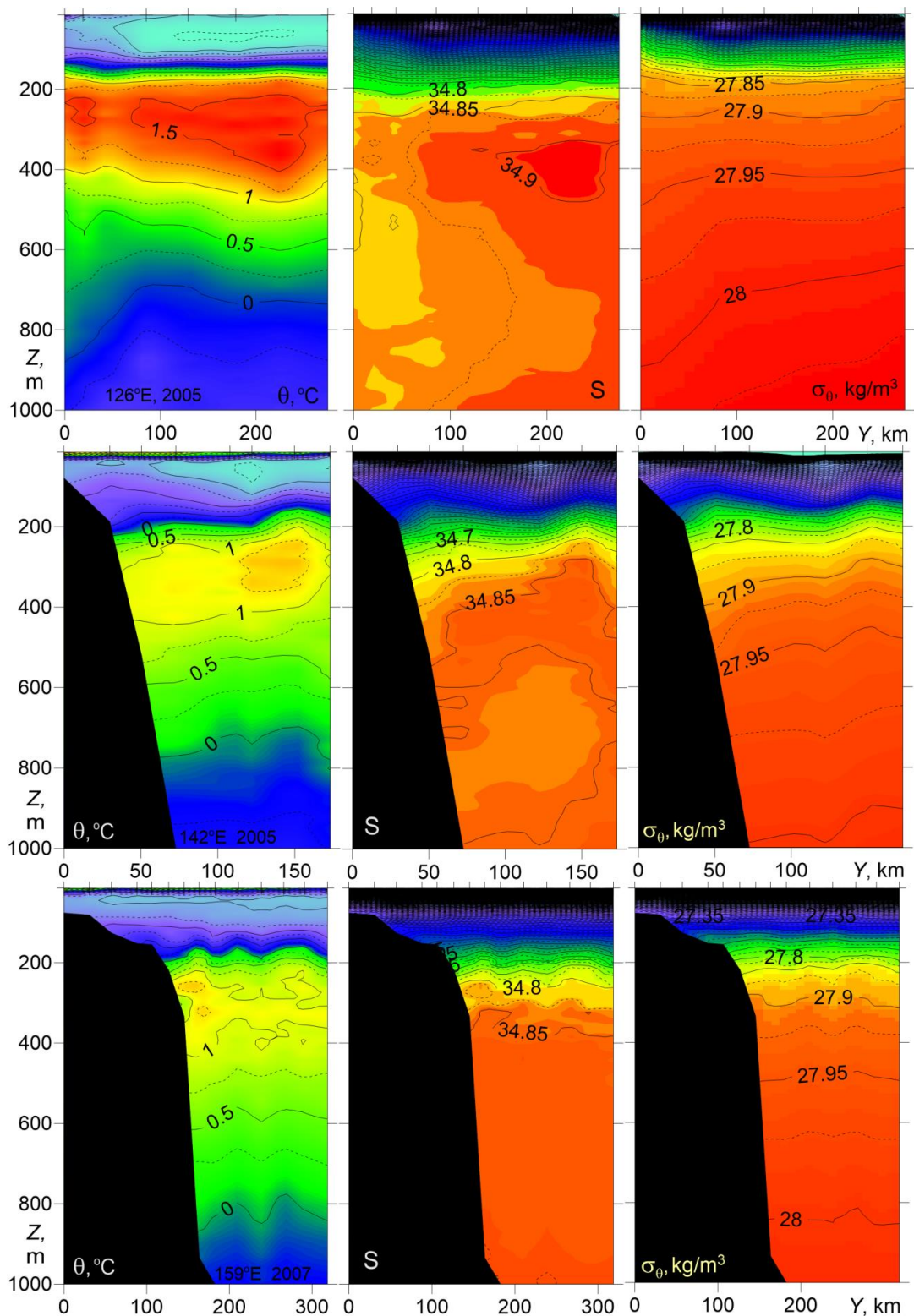
210

in the depth range close to 1000 m, and are ~~practically~~ absent at the depths above 950 m. The isopycnic surfaces in the bottom panel of Fig. 5 are relatively flat, indicating weak geostrophic flow (see Section 3.2). ~~Note that, the water with absolutely~~ The “absolutely stable” thermohaline stratification is ~~well visualized~~ below the temperature maximum with temperature decreasing and salinity increasing with depth (Fig. 5, bottom panel): ~~the temperature decreases and salinity increases with depth.~~ This feature of the mean thermohaline stratification is common to the Upper Polar Deep Water (UPDW) layer (Rudels et al., 1999).

215
220
225
In Fig. 6 three transects are presented, ~~two of which were made~~ at 126°E and 142°E (NABOS-2005) and ~~the third one was made~~ in the Makarov Basin at 159° E (NABOS-2007). On the transect along 126°E large slopes of isopycnic surfaces are observed, which corresponds to a fairly ~~intensive~~ strong geostrophic flow (see Section 3.2), confined to the depth range of 200–400 m, that is, to the area occupied by the FSBW. At the 142°E transect ~~which is located~~ on the Lomonosov Ridge, and at the 159°E transect in the Makarov Basin, the FSBW can be still identified as a warm layer ~~within a depth range of~~ between 200 and 400 m, where the maximum temperature is reduced to 1.49 °C and 1.42 °C, respectively (Fig. 6). The 142°E transect implies some eastward geostrophic transport, whereas at the 159° E transect, and in the area of cold waters (~~the depth range~~ below 800 m) in the sections shown in Fig. 6, the baroclinic flow is weak or absent.



230 Fig. 5. Temperature θ , salinity S , and potential density anomaly σ_θ versus distance and depth for cross-shelf transects at 103°E (upper) and 142°E (lower) (NABOS-09).



235 Fig. 6. Temperature θ , salinity S , and potential density anomaly σ_θ versus distance and depth for cross-shelf transects at 126°E, 142°E (top and middle, NABOS-2005) and 159°E (bottom, NABOS-2007).

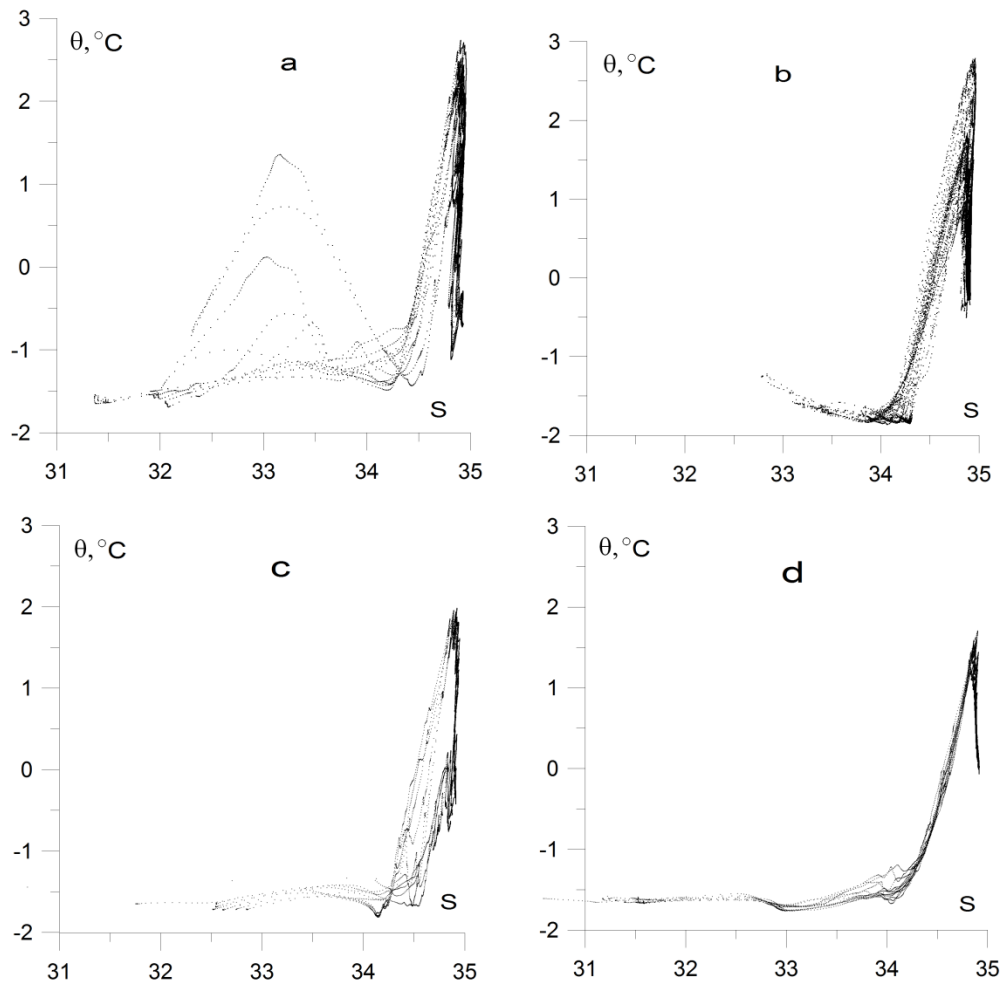
In summary, the a combined FSBW-BSBW structure with isopycnals sloping down to the north (from the slope), is typical for the longitude range 94–107°E. On In the transects made along 126°E, 142°E, and 159°E, the slopes of isopycnic surfaces sloping isopycnals indicating

240 ~~the baroclinic flow~~, were observed generally in the depth range of 200–400 m, that is in the area occupied by the FSBW. As the FSBW moved along the continental slope of the Eurasian Basin, ~~a significant decrease of its core temperature was observed in the FSBW core~~ decreased, but could be identified at all transects, including the two transects in the Makarov Basin (159°E). The cold waters ~~on~~ in the transects along 126°E, 142°E and 159°E, which can be associated with 245 the BSBW, had a minimum temperature above -0.5 °C, were ~~observed in the depth range~~ located below 800 m, and had ~~a little effect on the spatial structure of~~ relatively flat isopycnic surfaces ~~and horizontal gradient of density~~.

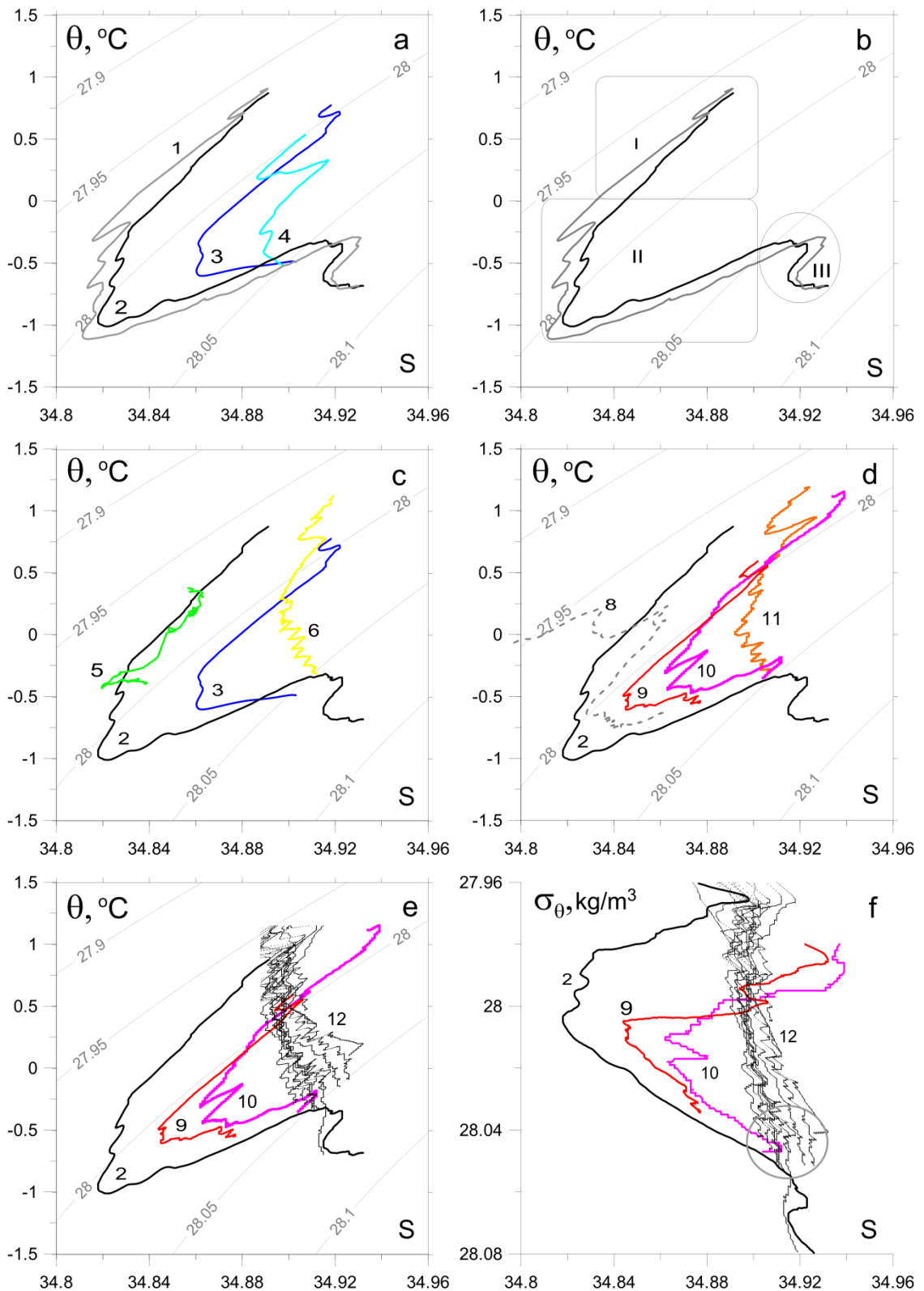
3.1.2 θ - S analysis

The difficulty in identifying the BSBW in the eastern part of the Nansen Basin is related to 250 the overlapping ranges of temperature and salinity inherent to the BSBW and the UPDW: -0.5 °C $< \theta < 0$ °C, and the salinity is close to 34.9 (Rudels et al., 1994; Walsh et al., 2007). It is also important to note that the BSBW in the St. Anna Trough mixes with the FSBW. Therefore, not only the cold Atlantic Waters, which are transported by the bottom gravity current, but also mixed warmer waters can enter the Nansen Basin through the trough (see Fig. 3). A detailed θ - S 255 analysis of different CTD sections can provide useful information on the transport and transformation of FSBW and BSBW. ~~Note that a pronounced~~ A distinct θ - S signal signature clearly indicates that the water mass has entered the area of observation. The absence of a signal a signature on the theta- S space indicates ~~one of the following: a) either~~ the water mass did not enter the area of observation; b) ~~it entered the area of observation being highly~~ or was 260 transformed, ~~namely, mixed~~ after mixing with other waters.

The differences in the behavior of the θ - S values are observed in the upper and deep layers of the Eurasian Basin and the St. Anna Trough (Fig.7). On the other hand, one cannot miss a similarity in the shape of the θ - S curves in the salinity range of 34.5–35.0. The similarity is obviously caused by the presence of FSBW. Fig. 7 demonstrates the transformation of the FSBW 265 and BSBW moving along the continental slope of the Eurasian Basin. More detailed information on the BSBW transformation can be extracted from θ - S diagrams presented in Fig. 8.



270 Fig. 7. θ - S diagrams based on the CTD profiling in (a) the St. Anna Trough (NABOS-09, 82° N), (b) the PS-96 section at 92°E, and the NABOS-09 sections at 103°E (c) and 142°E (d). For convenience of presentation, the points of the θ - S curves with salinity below 30 were ~~dropped~~ excluded.



275 Fig. 8. Thermohaline values of the BSBW and FSBW: a) based upon the CTD profiles, obtained in the St. Anna Trough (NABOS-09, section 82°N), curves 1–4 correspond to the stations (st.) 76, 78, 83 and 80, respectively; b) the same as “a” but only curves 1 and 2 are presented; regions I, II, III illustrate three different water masses in accordance with (Dmitrenko et al., 2015); for explanation see the text; c) based upon the section of PS-96, curves 5 and 6 corresponding to st. 32 and 42, respectively (depth range 600–1000 m), curves 2 and 3 are shown for the reference;

280 d) for CTD profiles at the 103°E section, NABOS-09, curve 8 (st. 64), curve 9 (st. 63), curve 10 (st. 62), curve 11 (st. 60), and curve 2 for the reference (see Fig. 5 for the location of the stations); e) based upon the CTD profiles in the depth range 500–1200 m measured at the 126°E (section of NABOS-09), curves 12; curves 2, 9 and 10 are shown for the reference; f) the same as “e” but presented in coordinates σ_θ, S .

285 The θ - S curves marked as 1 and 2 in Fig.8a correspond to stations 76 and 78, respectively, which were located at the eastern slope of the St. Anna Trough just in the near-bottom gravity current carrying the BSBW, while the curves marked as 3 and 4 correspond to stations 83 and 80 located near the mid-point (thalweg) of the trough in the western periphery of the gravity current (the location of the stations is shown in Fig. 3). To visualize ~~better~~ the BSBW transformation
290 **better**, the points of θ - S curves in the temperature and salinity ranges of $\theta > 1.2$ °C and $S < 34.76$, respectively, were omitted. Similar θ - S curves in the St. Anna Trough were observed within NABOS Program in other years (NABOS-13, NABOS-15).

The curves 1 and 2 in Fig. 8a have similar knee-like shape (Dmitrenko et al., 2015) formed by (i) the upper warm and saline water layer of the FSBW ($\theta \gg 0$ °C), (ii) the intermediate
295 colder and fresher water layer of BSBW ($\theta < 0$ °C) underlying the FSBW, and (iii) the denser, warmer and saltier “true” mode of the BSBW ($\theta \approx 0$ °C), see Fig. 8b: FSBW (region I), BSBW (region II), “true” mode BSBW (region III). ~~The difference between~~ The BSBW and **differs from the** “true” mode BSBW ~~is in that the former,~~ **and** is more diluted with the colder and fresher Barents Sea water (for more details see ~~paper by~~ Dmitrenko et al., 2015). We will be
300 interested in the transformation of the main part of the knee (region II), namely the transformation of BSBW.

In Fig. 8c the comparison of typical θ - S curves related to the St. Anna Trough (they are also shown in the other panels of Fig. 8 for reference) with that of the 92°E section of PS-96 is given: the curves 5 and 6 correspond to st. 32 and st. 42 (depth range 600–1000 m) of the PS-96
305 section, respectively. St. 32 was located next to the slope, while st. 42 was located about 250 km apart from the slope. The coincidence of curve 5 with a part of curve 2 ~~evidences for the~~ **implies a BSBW moving flow** along the slope of Nansen Basin (see Fig. 4 and its legend 1). Curve 6 corresponds to the UPDW. The θ - S diagrams for CTD profiles at the section 103°E are presented by curves 8-11-(see Fig. 5 for the locations of stations). Curves 8, 9, and 10 are similar to curve
310 2, and indicate the BSBW. Curve 11, ~~being~~ similar to curve 6 in Fig. 8c, corresponds to ~~the θ - S values of the~~ UPDW. However, the BSBW is not observed ~~in the section at~~ 126°E: see Fig. 8e, where a collection of θ - S curves (collectively referred as 12) presents all CTD profiles in the depth range 500–1800 m measured at ~~the section~~ 126°E of NABOS-09. Also we do not observe

the BSBW further to the east on the section 142°E section of NABOS-09 (not shown) as well as
315 or in the Makarov Basin.

To estimate the potential density of deep waters at the sections 103°E and 126°E σ_θ - S
diagrams are shown in Fig. 8f: curves 2, 9 and 10 correspond to θ - S curves 2, 9 and 10 presented
in Fig. 8d, curves 12 correspond to curves 12 in Fig. 8e. As one can see, t The BSBW at 103°E
and 126°E is also characterized by a knee-shape diagram also in coordinates in σ_θ , S coordinates
320 (Fig. 8f, numbers correspond to those in other panels) . However the knee-shape diagram is not
observed along 126°E (curve 12) in these coordinates. The dense and cold deep waters in the
section 126°E have σ_θ , θ , S values typical for the “true” BSBW mode (Dmitrenko et al., 2015).
Nevertheless, it is hardly correct to consider these waters (see σ_θ , S values inside the circle; Fig.
8f) as the “true” BSBW mode, since σ_θ , θ , S values of these waters satisfactorily also correspond
325 to σ_θ , θ , S values of the UPDW characteristics hence cannot be distinguished as the “true”
BSBW mode. To evaluate the transformation of the “true” mode of BSBW an additional analysis
is required, which is beyond the scope of this paper.

The results presented in Fig. 8 show that t The BSBW signal which is characterized by the
knee-shape diagram in coordinates θ - S and σ_θ - S , is not visible at 126°E (Fig. 8). This is
330 consistent with the conclusion formulated in Subsection 3.1.1 that by 126°E the BSBW is not
accompanied by any noticeable perturbations tilt of isopycnals. Moreover, given the
characteristic feature of the θ - S structure of BSBW in the St. Anna Trough (curves 1–4 in Fig.
8a) was observed in other years, we carried out a similar analysis using all available CTD data
and found that the BSBW signal is either strongly weakened or not visible is not distinct
335 longitude (see Fig.9). The only exception was 2002, when the BSBW signal was still observed at
126°E. It suggests that the BSBW and FSBW begin to mix intensively immediately after 103°E.
However On the other hand, the FSBW signal is well identified at 126°E and further along the
slope of the Eurasian Basin (and even in the Makarov Basin), while we cannot say the same
about the BSBW signal. Thus, one may assume that east of 126°E the geostrophic volume flow
340 rate of the AW is mainly provided by the FSBW.

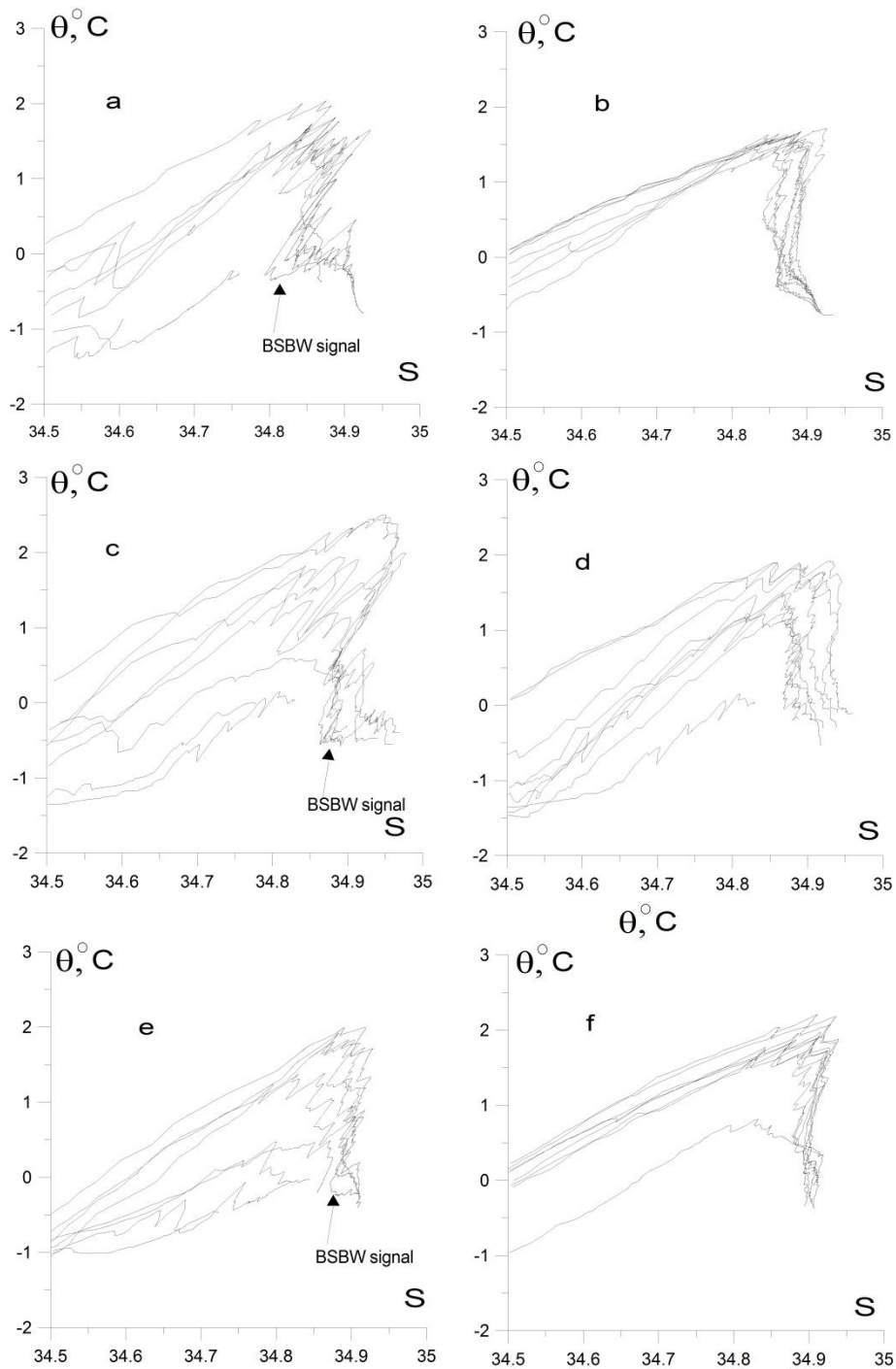


Fig. 9. θ -S diagrams based on the CTD profiling : NABOS-05: (a) and (b), 103°E (a), 126°E (b);
 345 NABOS-06: (c) and (d), 103°E (c), 126°E (d); NABOS-08: (e) and (f), 103°E (e), 126°E (f).

3.2 Characteristics of the Atlantic Water flow and geostrophic estimates of the volume flow rate

The estimates of **the geostrophic volume flow rate** V , as well as estimates of **and** the hydrological parameters describing the AW flow in the Eurasian and Makarov Basins, are presented in Table 1. The geostrophic estimates of the near-bottom ~~gravity~~ volume flow rate of the BSBW in zonal transects across the St. Anna Trough are presented in Table 2. The only

exception is the transect at 82°N, where the near-bottom gravity current with a considerable eastward component due to overflow across a sufficiently deep ridge (approx. 500 m deep) east of the St. Anna Trough (Fig. 3, top panels) makes the estimate of AW transport northward questionable. Note also that ~~prior to the BSBW entering the area of the Eurasian Basin to the west of the St. Anna Trough~~ our estimates refer to the FSBW; to east of this region ~~BSBW enters the Eurasian Basin and~~ our estimates should be attributed to the joint contribution of ~~the two branches —the FSBW and BSBW— to the transfer of the AW~~ (FSBW and BSBW).

The hydrological parameters shown in Table 1 can be interpreted as follows. The maximum water temperature of the AW may exceed 5 °C in cases when the AW inflow to the Eurasian Basin consists of especially warm water masses. Typical changes in the maximum temperature and salinity ~~maxima~~ of the AW moving along the slope over a distance of about 1000 km are approximately 1–2 °C and 0.1, respectively. ~~Such values of the maximum temperature of the AW~~ These changes lead to a slight increase in potential density and therefore a deviation of the AW from the isopycnic distribution ~~should~~ can be expected. This effect is ~~These changes are~~ most likely associated with the exchange of heat, salt, and mass with the surrounding waters ~~due to the formation of~~ through intrusive layering and ~~the influence of double diffusion (on the observation and study of intrusions in the Arctic Basin see, e.g., Rudels et al., 1999; Kuzmina et al., 2011; Polyakov et al., 2012; Kuzmina et al., 2018) and also with the AW core transformation by sea ice melting and cooling (Rudels, 1998).~~ The intrusions, in particular, can also contribute to the reduction of the AW heat and salt content and the volume flow rate. The differences in the AW heat and salt content and the volume flow rate can be clearly seen from the PS-96 section when comparing data from stations near the continental slope of the Eurasian Basin at 92°E and from the vicinity of the Lomonosov Ridge at 140°E.

It is worth noting that the maximum value of the AW temperature (θ_{max}) ~~according to the presented in this data set~~ is always observed in the upper layer of the Eurasian Basin at the depths below the density jump layer ~~pycnocline~~ but not exceeding 350 m, while the maximum salinity (S_{max}) at sections in the eastern part of the Basin can be observed at depths greater than 1000 m.

$X_{\theta_{max}}$ in Table 1 is the distance of the AW core (which can be associated with θ_{max}) from the slope/shelf boundary. The highest value and the maximum variation of this parameter is observed near 126°E and 142°E, where a two-core structure of AW is often observed (Pnyushkov et al., 2015).

The noticeable increase of θ_{max} in 2006 at 31°E and 103°E and the intensive warming of the AW were first reported in (Polyakov et al., 2011). The present results show that the increase

of the temperature of the AW in 2006 was also accompanied by an increase of volume transport (see Table 1, the section along 103°E and reasonings below). This can be caused not only by the warming of the AW, but also by an increased inflow of the AW to the Eurasian Basin.

The ~~evaluations of geostrophic current~~ transport in the range of 31–159°E ~~are~~ **is**
390 characterized by a high variability (Table 1). This may be due to ~~the following reasons:~~ a) the
~~deviation of some sections from the normal~~ **a) a section orientation oblique** to the current; b) the
difference in the horizontal scales of the sections; c) ~~some~~ uncertainty in the choice of the
reference level for geostrophic calculations; d) meandering of the flow; e) the effect of synoptic
quasi-geostrophic eddies on the flow volume rate. ~~All of these reasons contribute some noise to~~
395 ~~the resulting volume flow rate estimates.~~ In order to find statistically consistent estimates of the
variability of geostrophic volume flow rate along the slope of the basin based on a limited
~~material~~ **data set**, the following was done. The volume flow rates obtained for all sections within
the range 31°–92 °E for different years were used to calculate the mean volume flow rate (region
I; the number of volume flow rate values ~~to be~~ averaged is $N = 6$). Similarly, the average volume
400 flow rate was calculated for the region 94°–107°E (region II; $N = 9$). The remaining average
estimates of geostrophic volume flow rate were calculated for sections 126°E (region III; $N = 9$),
142°E (region IV; $N = 10$) and 159°E (region V; $N = 2$). Then the ~~confidence intervals with a~~
~~probability of 95% (typical confidence interval) and 80% (acceptable confidence interval for~~
~~working with a limited statistical material)~~ **confidence intervals** were determined using the
405 Student t-distribution. All estimates of average volume flow rates and confidence intervals are
presented in Tables 1 and 2.

~~The above mean estimates allow us to conclude that~~ **On the average**, the volume flow rate
increases from region I to region II, then decreases to region III and ~~after that decreases to~~ region
IV, followed by a sharp decrease in region V. However, ~~the 95% confidence intervals validate~~
410 ~~only the difference between the volume flow rate in region II and the values in regions IV and V~~
are significant at 95% confidence. **Transport values bounded by the** confidence intervals for
regions II, IV and V are (0.46; 1.72), (0.12; 0.44) and (-0.37; 0.43), respectively. These intervals
indicate that the mean volume flow rate in region II exceeds the value of the same parameter in
regions IV and V with a high probability of 95%. The 80% confidence intervals overlap only for
415 regions III and IV, (0.25; 0.53) and (0.18; 0.38), respectively. In this regard, ~~we can declare that~~
~~the above described~~ **the** change in the volume flow rate along the slope is **reliable significant**
with a probability of 80%, except for changes in volume flow rate from region III to region IV.

The above values of the mean volume flow rate and confidence intervals also suggest that
the increase in volume flow rate in 2006 ~~was caused by the climate impact~~ **is significant**, and not

420 **caused** by the “noise” in the data. Indeed, the volume flow rates in regions II, III, and IV in 2006 exceeded the upper limits of the corresponding 95% confidence intervals. From statistical point of view such a significant increase in volume flow rates at the same time in three regions is a very rare event that can hardly be explained by random “noise” in the data caused, for example, by the influence of synoptic eddies.

425 Let us turn our attention to the following features of the volume flow rate estimates: high volume flow rate estimates at 96°E, 103°E, 107°E, a negative volume flow rate estimate at 126°E in 2013 and low volume flow rate estimates at 31°E, 98°E in 2009 (Table 1). Indeed, the AW volume flow rate in the BSBW area of entry into the Eurasian Basin in 2013 was almost equal to the maximum volume flow rate in 2006 (103°E) and was quite high up to the longitude
430 107°E. This phenomenon as well as the intense warming in 2006 can be associated with the ~~impact of climate~~ **recent changing** conditions **in the Arctic**. ~~The~~ **We hypothesize that the** negative volume flow rate at 126°E was, ~~according to the authors, due to~~ **because of** the influence of local return flows which can be observed near the slope (Pnyushkov et al., 2015). Low FSBW volume flow rate estimates in 2009 are probably associated with a strong deviation of the flow from the
435 slope, which may ~~have been resulted in an underestimation of~~ **underestimate** the AW volume flow rates **transport** due to the small length of the ~~euts~~ **transects** to the north (see also **Section 4** below). ~~Another reason may be a sharp decrease in the intensity of the flow of the AW through the Fram Strait that most likely took place that year.~~

~~It is important to analyze average values of volume flow rate V_{mean} in region I and in the St.~~
440 ~~Anna Trough.~~ The mean value of the FSBW volume flow rate **in region I** is $V_{mean} = 0.5$ Sv. This estimate of volume flow rate is about half the estimate of the BSBW mean volume flow rate, $V_{mean} = 0.79$ Sv ($N = 3$, Table 2). (The **difference is significant at** 80% confidence intervals ~~do not overlap indicating that the BSBW volume flow rate does exceed the FSBW volume flow rate~~). The BSBW mean volume flow rate exceeding nearly twice the FSBW mean volume flow rate results in a dominance of the BSBW pattern of potential density contours in the longitude
445 range of 94–107°E (region II), where both branches of the AW are present. Moreover, the sum of the mean values of the FSBW and the BSBW volume flow rate geostrophic estimates, $V_{mean} = 0.5 + 0.79 = 1.29$ Sv, corresponds well ~~to the mean geostrophic estimate of volume flow rate for~~ **with** the combined FSBW and BSBW flow within the region II: $V_{mean} = 1.09$ Sv. Thus, the
450 increase in geostrophic ~~volume flow rate~~ **transport** in region II is mainly due to the influence of the BSBW. ~~It should be noted that, according to sections 3.1.1 and 3.1.2, t~~ The decrease in geostrophic volume flow rate in region III can also be associated primarily with the BSBW,

namely, with the decrease in the BSBW signal transport in the 126°E section and further along the slope (see sect. 3.1.1 and 3.1.2).

455 Finally, at the section 159°E located section in the Makarov Basin, the geostrophic estimate of the along-slope volume flow rate of mixed waters of the FSBW and the BSBW has further greatly reduced down to $V_{mean} = 0.03$ Sv ($N = 2$), which is of more than one order of magnitude smaller than that in the Nansen and Amundsen Basins. Despite the low statistical significance of the latter estimate (due to small value of $N = 2$) one may conclude that the major part of the AW entering the Arctic Ocean circulates cyclonically within the Nansen and Amundsen Basins, and only its small part flows to the Makarov Basin (Rudels et al., 2015; Rudels, 2015). However, additional studies using more CTD data are required to confirm this result.

465 Table 1. Characteristics of the Atlantic Water flow in the course of its propagation along continental slope of the Eurasian Basin of the Arctic Ocean. *Dist* is the along-slope distance from the Fram Strait; θ_{max} is the maximum temperature; $\sigma_{\theta}(Z_{\theta max})$, $S(Z_{\theta max})$, $Z_{\theta max}$, and $X_{\theta max}$ are the values of potential density, salinity, depth, and lateral displacement from the slope for the point θ_{max} ; S_{max} and Z_{Smax} are the same as θ_{max} and $Z_{\theta max}$ but for the salinity maximum salinity and depth of S_{max} ; V is the geostrophic estimate of the volume flow rate. The mean values and 95% / 80% confidence intervals of the volume rate, V_{mean} , calculated separately for CTD transects at 470 31–92°E, 94–107°E, 126°E, 142°E and 159°E, are presented too also shown. The last row in the Table presents the characteristics of the return flow of the AW by the Lomonosov Rigde at the longitude 140°E and latitude 86.5°N (PS96, see Fig. 1). Year is given in the first column (e.g. NABOS06 corresponds to 2006).

<i>Exp</i>	<i>Lon</i> [°E]	<i>Dist</i> [km]	θ_{max} [°C]	$\sigma_{\theta}(Z_{\theta max})$ [kg/m ³]	$S(Z_{\theta max})$	$Z_{\theta max}$ [m]	$X_{\theta max}$ [km]	S_{max}	Z_{Smax} [m]	V [Sv]
NABOS06	31	404	5.670	27.579	34.980	42	-11	35.099	72	0.57
NABOS08	31	404	4.883	27.771	35.103	101	0	35.105	176	0.80
NABOS09	31	404	3.691	27.818	34.999	89	0	35.002	91	0.10
NABOS09	60	856	2.503	27.891	34.951	175	10	34.981	363	0.47
NABOS13	90	1290	2.600	27.903	34.975	250	41	34.996	333	0.46
PS96	92	1322	2.786	27.875	34.960	271	33	34.968	329	0.58
$V_{mean} = 0.50 \pm 0.24 / \pm 0.14$ Sv										
NABOS15	94	1355	2.445	27.946	35.012	331	33	35.015	365	0.47
NABOS13	96	1388	2.548	27.902	34.969	207	70	34.978	264	2.06
NABOS09	98	1421	2.300	27.906	34.948	220	79	34.971	345	0.09
NABOS05	103	1561	2.029	27.870	34.876	179	39	34.934	309	0.32
NABOS06	103	1561	2.528	27.888	34.950	220	50	34.978	260	2.23
NABOS08	103	1561	1.980	27.886	34.891	201	60	34.929	325	0.42
NABOS09	103	1561	1.984	27.913	34.925	244	50	34.951	365	0.87
NABOS13	103	1561	2.278	27.904	34.942	215	80	34.956	419	1.59
NABOS13	107	1695	1.903	27.937	34.945	359	120	34.948	404	1.77
$V_{mean} = 1.09 \pm 0.63 / \pm 0.38$ Sv										
NABOS02	126	2104	1.406	27.938	34.902	324	243	34.932	2061	0.05
NABOS03	126	2102	1.341	27.941	34.899	336	342	34.921	1886	0.41
NABOS04	126	2102	1.770	27.906	34.896	271	87	34.925	2431	0.61

NABOS05	126	2102	1.695	27.936	34.926	359	227	34.935	2841	0.75
NABOS06	126	2102	1.905	27.923	34.930	284	193	34.960	968	0.77
NABOS07	126	2102	2.085	27.907	34.928	266	242	34.942	340	0.60
NABOS08	126	2102	2.195	27.885	34.911	206	235	34.939	365	0.31
NABOS09	126	2102	1.907	27.909	34.913	316	33	34.932	1018	0.40
NABOS13	126	2102	1.946	27.937	34.949	346	228	34.951	428	-0.21
NABOS15	126	2102	1.653	27.918	34.898	246	400	34.942	3816	0.22
$V_{mean} = 0.39 \pm 0.22 / \pm 0.14$ Sv										
NABOS03	142	2456	1.089	27.912	34.841	269	41	34.862	1000	0.06
NABOS04	142	2456	1.401	27.909	34.865	281	0	34.907	1608	0.21
NABOS05	142	2456	1.492	27.906	34.870	284	100	34.906	1550	0.26
NABOS06	142	2456	1.981	27.874	34.876	234	111	34.960	1016	0.60
NABOS07	142	2456	1.855	27.879	34.870	231	0	34.920	2064	0.09
NABOS08	142	2456	1.599	27.915	34.890	260	200	34.908	347	0.23
NABOS09	142	2456	1.704	27.915	34.900	253	101	34.917	1082	0.22
NABOS13	142	2456	1.475	27.940	34.909	331	115	34.926	1150	0.18
NABOS15	142	2456	1.353	27.936	34.892	326	106	34.913	1372	0.63
$V_{mean} = 0.28 \pm 0.16 / \pm 0.10$ Sv										
NABOS07	159	2783	1.424	27.887	34.839	255	0	34.880	1075	-0.01
NABOS08	159	2783	1.383	27.893	34.843	245	0	34.889	1266	0.06
$V_{mean} = 0.03 \pm 0.40 / \pm 0.10$ Sv										
PS96back	140E 86.5N	3178	1.812	27.890	34.880	219	≈ 700	34.902	472	-0.09

475

Table 2. Geostrophic estimates of the volume flow rate for near-bottom gravity flow of the Barents Sea Branch of Atlantic Water (BSBW) on zonal transects across the St. Anna Trough. The uncertainty estimates are 95% and 80% confidence intervals.

<i>Exp</i>	NABOS09	NABOS13	NABOS15	
<i>Lat</i> [°N]	81.00	81.33	81.41	V_{mean}
<i>V</i> [Sv]	0.89	0.73	0.76	$0.79 \pm 0.22 / \pm 0.10$

480

3.3 Interannual variability of the AW temperature-salinity values and the volume flow rate

Within the NABOS project, in accordance with Table 1, the cross-slope CTD transects at 103°E, 126°E, and 142°E were repeatedly performed for a number of annual campaigns (Table 1): 2005, 2006, 2008 and 2013 (103°E), 2002–2009, 2013 and 2015 (126°E), 2003–2009, 2013, and 2015 (142°E). We use the repeated transects may contain some information on to describe the inter-annual variability of the AW, and we attempted to explore such a possibility.

Time series of the maximum temperature of the AW temperature maximum, θ_{max} , and the related values of salinity $S(\theta_{max})$ and potential density anomaly $\sigma_{\theta}(\theta_{max})$ (Fig. 10) show that the period of 2006 to 2008 was characterized by not only an increased temperature of the AW in the eastern part of the Eurasian Basin, but an increased salinity and density reduction. The temperature excess during this period was as large as 0.6–1.0 °C relative to 2002–2003 and 0.3–0.6 °C relative to 2013–2015. The time series of corresponding values of salinity $S(\theta_{max})$

490

displayed in 2006 local maxima at the transects 126°E and 142°E, and the absolute maximum at the transect 103°E; the salinity excess for the maxima largely decreased with the longitude from approximately 0.06 at 103°E to less than 0.01 at 142°E. In accordance with our analysis the time series of θ_{max} had a maximum in 2013 but only at 103°E (see Table 1 and Fig.10). The time series of $S(\theta_{max})$ display a trend of an increase of AW salinity in 2006–2008 and 2013 also over time, that can be referred to as a AW salinization in early 2000s. The change of salinity of AW at 142°E in time also draws attention to the following aspect: the salinity increases almost monotonously in the period from 2003 to 2013. How can such behavior of salinity be explained? The mechanism behind this salinity evolution is not clear. It is also worth noting that the maxima of θ_{max} and $S(\theta_{max})$ in 2006 and 2013 (at 103°E) were accompanied by the volume flow rate high maxima in transport.

4 Discussion

Here we discuss the following issues: a) differences in the identification of the BSBW; b) a comparison of the geostrophic volume flow rate estimates with other studies; c) the weakening of the BSBW signal at 126 °E and further east.

a) Advection and interaction of waters with different θ - S characteristics in the Arctic Basin, as well as the impact of climate change that has been observed over the past decade (Polyakov et al., 2017) complicate an accurate identification of water masses. However, a robust approach to the determination of the FSBW and BSBW, which was proposed in Dmitrenko et al. (2015), is effective for distinguishing the water masses of these AW the FSBW and BSBW branches. As an exception, this approach does not take into account some cases, namely fails when the FSBW temperature is below 0 °C (see Fig. 2 in Dmitrenko et al., 2015), and/or the BSBW temperature is close to 1 °C (see Fig. 6 in Schauer et al., 2002a). If such cases are rare, then either of the two approaches can be used to identify the BSBW and FSBW. Indeed, the identification of the BSBW on the PS-96 section in our case (we used the approach proposed by Dmitrenko et al., 2015; see paragraph 3.1.1) does not differ much from that proposed by Schauer et al. (2002b). However, these discrepancies can lead to almost an order of magnitude difference in estimates of the volume flow rate of the BSBW only due to the differences in the BSBW cross-sectional area.

b) Based on the velocity measurements with moored instruments (1997–2010) in the area of the West Spitsbergen Current (WSC) near the Fram Strait (zonal transect at ~78°50' N), it was found that approximately 3 Sv of the AW flows into the Nansen Basin (Beszczynska-Möller et al., 2012). The long-term mean volume transport confined to the WSC core branch (or Svalbard

branch in accordance with Schauer et al., 2004) included 1.3 ± 0.1 Sv of the AW warmer than 2°C . The offshore WSC branch (or Yermak branch) carried on average 1.7 ± 0.1 Sv of the AW. Investigation of water transport in and north of the Fram Strait based upon CTD measurements on zonal and meridional sections have been done by Marnela et al. (2013). The variability range of the estimates of the AW geostrophic transport of the Svalbard branch was calculated for meridional sections made in from 1997, 2001, and 2003 (summer/fall), and was between 0.06 Sv and 0.7 Sv (Marnela et al., 2013). In Kolås and Fer (2018) observations of the oceanic current and thermohaline field (in summer 2015) in the three sections were used to characterize the evolution of the WSC along 170 km downstream distance. Absolute geostrophic transports of AW were calculated on the basis of absolute geostrophic velocities and it was shown that ranged from 0.6 Sv to 1.3 Sv of the AW is carried by in the Svalbard branch. In accordance with earlier studies of the currents in the Fram Strait, recirculation of the AW can be significant, and the volume flow rate of the AW entering the Arctic Ocean can be equal only 1 Sv (Rudels, 1987), or it ranges from 0.6 Sv to 1.5 Sv (Rudels, 1987; Aagaard and Carmack, 1989).

Our estimate of the mean volume flow rate V_{mean} in region I (31° – 92°E) is in the range of variation in the above estimates. However, the upper confidence limit of our estimate does not reach 1 Sv. Moreover, we used the inequality $T > 0^\circ\text{C}$ to identify the AW while in Beszczynska-Möller et al. (2012) the volume flow rates of the AW entering the Eurasian Basin through the Fram Strait were determined from the for waters with $T > 2^\circ\text{C}$ condition. In this regard, we can admit that our assessment is somewhat underestimated. Probably, this may be due to the fact that Comparatively smaller transport in region I may be because the sections along the longitudes 31°E (see Fig. 1) are less than 100 km. Actually, at the sections along this longitude wide and do not cover the full extent of the FSBW (Fig. 2, upper panel) only a part of the FSBW is observed. Given that the volume flow rate estimate is sensitive the sensitivity to the definition of AW and the resulting to the accepted value of cross-sectional area of the AW (see issue point “a” above), the volume transport may be underestimated. One cannot also ignore the fact that horizontal density gradients of the geostrophic flow can be strengthened or weakened during It is possible that the formation and passage of synoptic eddies, the influence of which on the average density field cannot be filtered out leads to variability in transport rates. According to Perez-Hernandez et al. (2017) north of Svalbard (between 21° and 33°E) in September, 2013, a large difference was found in the estimates of geostrophic volume flow rate (from 0.53 Sv to 3.39 Sv) due to the passage of eddies and meandering of the current. Våge et al. (2016) based on geostrophic velocities at two CTD sections across the boundary current near 30°E (September, 2012) evaluated a net AW volume flow rate of 1.6 ± 0.3 Sv. Authors of this paper They found evidence

560 of a large eddy affecting the mean volume transport calculations. The barotropic velocity component, which is not taken into account in our estimates, can also ~~affect the values of the volume flow rates~~ contribute to larger transports. However, if the ice cover in the Eurasian Basin is high, the barotropic addition to the flow velocity in a stratified ocean hardly can play a decisive role in conditions with high ice concentration in the Eurasian Basin, we might expect a
565 reduced barotropic contribution from the sea level changes induced by wind forcing. In accordance to cruise reports, the NABOS CTD sections were characterized by the ice concentrations of 50–100% (see <https://uaf-iarc.org/nabos-cruises/>). Exceptions occurred in the near-slope areas of the Laptev Sea, that is, in the sections along $\sim 126^\circ\text{E}$, where the ice concentration varied from 0 to 100%, having a maximum value in the northern part of the
570 sections. In such areas, the contribution of the barotropic component to the flow velocity can be very significant large. For example, using long-term measurements (1995 – 1996) from a mooring in the near-slope area of the Laptev Sea, Woodgate et al. (2001) showed that the contribution of the barotropic component to the velocity of the Arctic Ocean Boundary Current (AOBC) was equal to the contribution of the first three baroclinic modes. To estimate
575 the volume flow rate they assumed that the Assuming an average velocity based on the measurements in the upper 1200 m layer was of 4.5 cm/s and the horizontal extension of the flow was a width of 50 to 84 km. At such values of the velocity and cross section of the flow the volume flow rate was estimated at 5 ± 1 Sv. This estimate differs from is larger than our average estimate of the AW volume flow rate along 126°E (0.39 ± 0.22 , Table 1) by an order of
580 magnitude. Such a difference can be explained not only by the absence of a barotropic contribution in our case, but also by the fact that we took into account the volume transport of AW only (i.e. the cold, low-salinity surface layer was excluded) and considered certain season (August and September). Indeed, according to long-term measurements at 6 moorings on a section along 126°E , the AOBC volume flow rate varied from 0.3 Sv to 9 Sv (Pnyushkov et al.,
585 2018 b). Such a wide range in volume flow rate estimates is probably due to a combined effect of seasonal variability and mesoscale eddies (Pnyushkov et al., 2018 a).

The fact that seasonal variations can in some cases significantly affect the AW volume flow rates (see also the discussion of different estimates of the AW volume flow rate in Pnyushkov et al., 2018 b) is confirmed by a number of observations (Schauer et al., 2002a; Beszczynska-Möller et al., 2012; Pnyushkov et al., 2018 b). For example, the volume flow rate of the AW in the northwestern part of the Barents Sea was 0.6 Sv according to velocity measurements in summer (Schauer et al., 2002a). This estimate agrees well with our estimate of the AW transport of AW in the St. Anna Trough, 0.79 ± 0.22 Sv (Table 2). However, the analysis of current velocity measurements in the winter season at the same section in the

595 northwestern part of the Barents Sea gives ~~gave~~ a completely different estimate of ~ 2.6 Sv (Schauer et al., 2002a).

c) According to Dmitrenko et al. (2009), the BSBW signal ~~is~~ can be satisfactorily identified at 142°E . However, a “pattern” in the θ - S diagram far from the place of the BSBW entry into the Eurasian Basin can be regarded as the BSBW signal, if it maintains the similarity with the “pattern” of the BSBW at the exit from the St. Anna Trough, that is, with the so-called “knee” (Dmitrenko et al., 2015). Our analysis showed that the “knee” is regularly observed at 103°E , while at 126°E it is either absent or weakens strongly and, weak or distorted. Apparently ~~this is quite natural,~~ This may be expected since the flow velocity is small, and the BSBW covers a distance from 103°E to 126°E for 1–2 years. However, despite of such a long travel time, Fram Strait branch is well identified not only at 126°E , but also further along the slope. ~~It seems acceptable to associate this situation with characteristic features of~~ This suggests stronger transformation and mixing of, primarily, the BSBW. The BSBW transformation can be due to various reasons, including mixing with the FSBW caused by thermohaline intrusive layering at absolutely stable stratification (Merryfield, 2002; ~~Kuzmina et al., 2013;~~ Kuzmina et al., 2014; Kuzmina, 2016, Zhurbas N., 2018; Kuzmina et al., 2018, 2019). ~~Indeed, the intrusive layering in the ocean influences the processes of exchange and mixing of various water masses (see, e.g., Stern, 1967; Fedorov, 1976; Joyce, 1980; Zhurbas et al., 1993; Rudels et al., 1999; Kuzmina, 2000; Walsh and Carmack, 2003). Other reasons for the BSBW signal disappearance may be:~~ , the influence of the slope topography, the impact of local counterflows near the slope (see, for example, Pnyushkov et al., 2015), lateral convection (Ivanov and Shapiro, 2005; Ivanov and Golovin, 2007; Walsh et al., 2007), the impact of the Arctic Shelf Break Water (Aksenov et al., 2011; Ivanov and Aksenov, 2013) and mixing due to eddies (Schauer et al., 2002; Dmitrenko et al., 2008; Aagaard et al., ~~2012–~~2008; Pnyushkov et al., 2018a). The understanding of the processes of transformation and mixing of the BSBW and FSBW is necessary to verify an important concept proposed by Rudels, et al. (2015) that the BSBW supplies the major part of the AW to the Amundsen, Makarov and Canadian Basins, while the FSBW remains almost fully in the Nansen Basin.

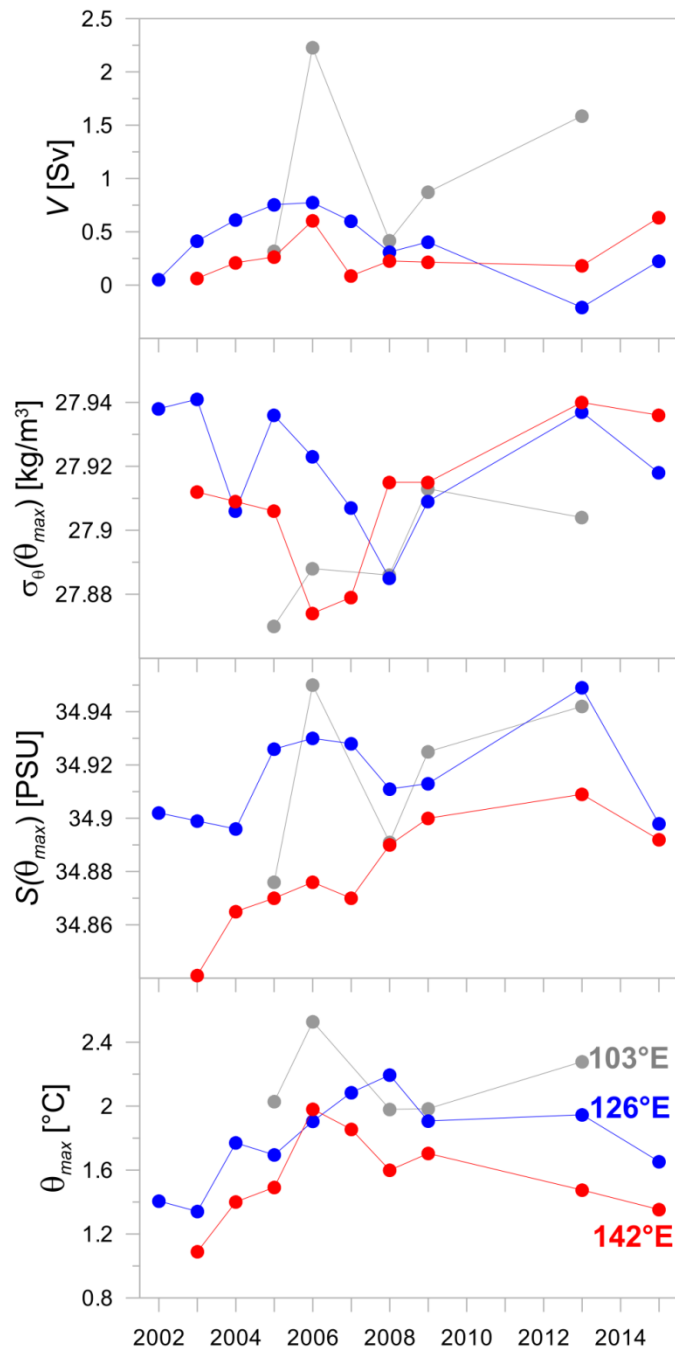
5 Summary

The θ - S properties and the volume flow rate estimates of the current carrying the AW in the Eurasian Basin and St. Anna Trough were obtained based on the analysis of CTD data collected within the NABOS program in 2002–2015; additionally CTD transect PS-96 was considered. ~~All estimates are given in tabular form.~~

FSBW was present at all transects, including the two transects in the Makarov Basin (159°E), while the cold waters at the transects along longitudes 126°E, 142°E and 159°E, which
630 can be associated with the influence of the BSBW, were observed in the depth range below 800 m and had little effect on the spatial structure of isopycnic surfaces and horizontal gradient of density. It is shown using θ - S analysis that the BSBW signal, which is characterized by the knee-shape feature in coordinates θ , S and σ_θ , S (see Fig.8), is either strongly weakened or not visible at the longitude 126°E (excluding the observations in 2002 at 126 °E), while the FSBW signal is
635 well identified at 126°E and further along the slope of the Eurasian Basin. Based on the revealed features of the temperature, salinity and density fields, it is suggested that east of 126°E the geostrophic volume transport of AW is mainly provided by the FSBW.

~~In order to assess spatial variability of the AW geostrophic volume flow rate, standard statistical analysis was used. It is shown with a 80% probability that t~~
640 ~~flow rate~~ of AW increases (with 80% confidence) from the region of 31°E–92°E (0.5 ± 0.14 Sv) to the region of 94°E–107°E (1.09 ± 0.38 Sv), then decreases to the region of 126°E (0.39 ± 0.14 Sv) and becomes small (0.03 ± 0.1 Sv) in the Makarov Basin (159°E).

The temporal variability of hydrological parameters and of the AW volume flow rate is summarized as follows. The time series of θ_{max} had an absolute maximum in 2006–2008 that can
645 be interpreted as a result of heat pulse in the early 2000s (Polyakov et al., 2011). In accordance with our analysis the time series of θ_{max} had a maximum in 2013 but only at the longitude 103°E (Table 1 and Fig.10). The time series of $S(\theta_{max})$ display a trend of an increase of AW salinity in 2006–2008 and 2013 also over time, that can be referred to as a AW salinization in early 2000s. Moreover the salinity increases almost monotonously in the period from 2003 to 2013 at 142°E .
650 It is important to underline also that the maxima of θ_{max} and $S(\theta_{max})$ in 2006 and 2013 (103°E) are accompanied by the volume flow rate highs. A significant increase in geostrophic volume flow rate identified in 2006 is shown to be caused by climate impact.



655 Fig. 10. Interannual variability of the maximum temperature θ_{max} and the related values of salinity $S(\theta_{max})$, potential density anomaly $\sigma_{\theta}(\theta_{max})$ and volume flow rate V on the cross-slope transects at 103°E, 126°E and 142°E.

Acknowledgments. This research, including the approach development, data processing and interpretation, performed by Nataliya Zhurbas, was funded by Russian Science Foundation, project no. 17-77-10080. Natalia Kuzmina (θ - S analysis, statistical analysis, participation in
660 discussion) was supported by the state assignment of the Shirshov Institute of Oceanology RAS (theme no. 0149-2019-0003).

The authors are very grateful to the NABOS group for providing the opportunity to use the CTD-data.

665 The authors are very grateful to the editor for evaluating the article and help in the work on the text and anonymous reviewers for useful comments.

References

- Aagaard, K.: On the deep circulation of the Arctic Ocean, *Deep-Sea Res.*, 28, 251–268, 1981.
- Aagaard, K., and Carmack, E. C.: The role of sea ice and other fresh water in the Arctic circulation, *J. Geophys. Res.*, 94(C10), 14485–14498, doi: 10.1029/JC094iC10p14485, 1989.
- 670 Aagaard, K., Andersen, R., Swift, J., and Johnson, J.: A large eddy in the central Arctic Ocean, *Geophys. Res. Lett.*, 35, L09601, doi: 10.1029/2008GL033461, 2008.
- Aksenov, Y., Ivanov, V. V., Nurser, A. J. G., Bacon, S., Polyakov, I. V., Coward, A. C., Naveira-Garabato, A. C., and Beszczynska-Moeller, A.: The Arctic Circumpolar Boundary Current, *J. Geophys. Res.*, 116, C09017, 1–28, doi:10.1029/2010JC006637, 2011.
- 675 ~~Arneborg, L., Fiekas, V., Umlauf, L., and Burchard, H.: Gravity current dynamics and entrainment—A process study based on observations in the Arkona Basin, *J. Phys. Oceanogr.*, 37, 2094–2113, doi:10.1175/JPO3110.1, 2007.~~
- Beszczynska-Möller, A., Fahrbach, E., Schauer, U., and Hansen, E.: Variability in Atlantic water temperature and transport at the entrance to the Arctic Ocean, 1997–2010, *ICES Journal of Marine Science*, 69(5), 852–863, doi: 10.1093/icesjms/fss056, 2012.
- 680 Dmitrenko, I. A., Kirillov, S. A., Ivanov, V. I., and Woodgate, R.: Mesoscale Atlantic water eddy off the Laptev Sea continental slope carries the signature of upstream interaction, *J. Geophys. Res.*, 113, C07005, doi: 10.1029/2007JC004491, 2008.
- Dmitrenko, I. A., Kirillov, S. A., Ivanov, V. V., Woodgate, R. A., Polyakov, I. V., Koldunov, N., Fortier, L., Lalande, C., Kaleschke, L., Bauch, D., Hölemann, J. A., and Timokhov, L. A.: Seasonal modification of the Arctic Ocean intermediate water layer off the eastern Laptev Sea continental shelf break, *J. Geophys. Res.-Oceans*, 114, C06010, <https://doi.org/10.1029/2008JC005229>, 2009.
- 685 Dmitrenko, I. A., Rudels, B., Kirillov, S. A., Aksenov, Y. O., Lien V. S., Ivanov, V. V., Schauer, U., Polyakov, I. V., Coward, A., and Barber, D. J.: Atlantic Water flow into the Arctic Ocean through the St. Anna Trough in the northern Kara Sea, *J. Geophys. Res.: Oceans*, 120(7), 5158–5178, doi: 10.1002/2015JC010804, 2015.
- 690 ~~Fahrbach, E., Meineke, J., Osterhus, S., Rohardt, G., Schauer, U., Tverberg, V., and Verduin, J.: Direct measurements of volume transport through Fram Strait, *Polar Res.*, 20(2), 217–224, doi: 10.1111/j.1751-8369.2001.tb00059.x, 2001.~~
- ~~Fedorov, K. N.: Physical Nature and Structure of Oceanic Fronts, *Gidrometeoizdat, Leningrad*, 296 pp., 1983 (in Russian).~~

- Ivanov, V. V., and Shapiro, G. I.: Formation of dense water cascade in the marginal ice zone in the Barents Sea, *Deep-Sea Res. Pt. I*, 52, 1699–1717, doi: 10.1016/j.dsr.2005.04.004, 2005.
- 700 Ivanov, V., and Golovin, P.: Observations and modelling of dense water cascading from northwestern Laptev Sea shelf, *J. Geophys. Res.*, 112, C09003, doi:10.1029/2006JC003882, 2007.
- Ivanov, V. V., and Aksenov, E. O.: Atlantic Water transformation in the Eastern Nansen Basin: observations and modelling, *Arctic and Antarctic Research*, 1(95), 72–87, 2013 (in Russian).
- 705 ~~Joyce, T. M.: A note on the lateral mixing of water masses, *J. Phys. Oceanogr.*, 7(4), 626–629, 1980.~~
- Kolås, E., and Fer, I.: Hydrography, transport and mixing of the West Spitsbergen Current: the Svalbard Branch in summer 2015, *Ocean Sci.*, 14, 1603–1618, doi: 10.5194/os-14-1603-2018, 2018.
- 710 ~~Kuzmina, N. P.: On the parameterization of interleaving and turbulent mixing using CTD data from the Azores Frontal Zone, *J. Mar. Syst.*, 23(4), 285–302, 2000.~~
- Kuzmina, N., Rudels, B., Zhurbas, V., and Stipa, T.: On the structure and dynamical features of intrusive layering in the Eurasian Basin in the Arctic Ocean, *J. Geophys. Res.*, 116, C00D11, doi: 10.1029/2010JC006920, 2011.
- 715 ~~Kuzmina, N. P., Zhurbas, N. V., and Rudels B.: Structure of intrusions and fronts in the deep layer of the Eurasian Basin and Makarov Basin (Arctic), *Oceanology*, 53(4), 410–421, doi: 10.1134/S0001437013040061, 2013.~~
- Kuzmina, N. P., Zhurbas, N. V., Emelianov, M. V., and Pyzhevich, M. L.: Application of interleaving Models for the Description of intrusive Layering at the Fronts of Deep Polar
- 720 Water in the Eurasian Basin (Arctic), *Oceanology*, 54(5), 557–566, doi: 10.1134/S0001437014050105, 2014.
- Kuzmina, N. P.: Generation of large-scale intrusions at baroclinic fronts: an analytical consideration with a reference to the Arctic Ocean, *Ocean Sci.*, 12, 1269–1277, doi: 10.5194/os-12-1269-2016, 2016.
- 725 Kuzmina, N. P., Skorokhodov, S. L., Zhurbas, N. V., and Lyzhkov, D. A.: On instability of geostrophic current with linear vertical shear at length scales of interleaving, *Izv. Atmos. Ocean. Phys.*, 54(1), 47–55, doi: 10.1134/S0001433818010097, 2018.
- Marnela, M., Rudels, B., Houssais, M.-N., Beszczynska-Möller, A., and Eriksson, P. B.: Recirculation in the Fram Strait and transports of water in and north of the Fram Strait derived
- 730 from CTD data, *Ocean Sci.*, 9, 499–519, doi: 10.5194/os-9-499-2013, 2013.
- Merryfield, W. J.: Intrusions in Double-Diffusively Stable Arctic Waters: Evidence for Differential mixing?, *J. Phys. Oceanogr.*, 32, 1452–1459, 2002.

- Pérez-Hernández, M. D., Pickart, R. S., Pavlov, V., Våge, K., Ingvaldsen, R., Sundfjord, A., Renner, A. H. H., Torres, D. J., and Erofeeva, S. Y.: The Atlantic Water boundary current north of Svalbard in late summer, *J. Geophys. Res.-Oceans*, 122, 2269–2290, <https://doi.org/10.1002/2016JC012486>, 2017.
- Pfirman, S. L., Bauch, D., and Gammelsrød, T.: The northern Barents Sea: water mass distribution and modification, in: *The Polar Oceans and Their Role in Shaping the Global Environment*, Geophysical Monograph 85, edited by: Johannessen, O. M., Muench, R. D., and Overland, J. E., American Geophysical Union, Hoboken, NJ, 77–94, 1994.
- Pnyushkov, A. V., Polyakov, I. V., Ivanov, V. V., Aksenov, Ye, Coward, A. C., Janout, M., and Rabe, B.: Structure and variability of the boundary current in the Eurasian Basin of the Arctic Ocean, *Deep-Sea Res. Pt. I*, 101, 80–97, <https://doi.org/10.1016/j.dsr.2015.03.001>, 2015.
- Pnyushkov, A. V., Polyakov, I. V., Padman, L., and Nguyen An T.: Structure and dynamics of mesoscale eddies over the Laptev Sea continental slope in the Arctic Ocean, *Ocean Sci.*, 14, 1329–1347, <https://doi.org/10.5194/os-14-1329-2018>, 2018a.
- Pnyushkov, A. V., Polyakov, I. V., Rember, R., Ivanov, V. V., Alkire, M. B., Ashik, I. M., Baumann, T. M., Alekseev, G. V., and Sundfjord, A.: Heat, salt, and volume transports in the eastern Eurasian Basin, *Ocean Sci.*, 14, 1349–1371, <https://doi.org/10.5194/os-14-1349-2018>, 2018b.
- Polyakov, I. V., Beszczynska, A., Carmack, E. C., Dmitrenko, I. A., Fahrbach, E., Frolov, I. E., Gerdes, R., Hansen, E., Holfort, J., Ivanov, V. V., Johnson, M. A., Karcher, M., Kauker, F., Morison, J., Orvik, K. A., Schauer, U., Simmons, H. L., Skagseth, Ø., Sokolov, V. T., Steele, M., Timokhov, L. A., Walsh, D., and Walsh, J. E.: One more step toward a warmer Arctic, *Geophys. Res. Lett.*, 32, L17605, doi: 10.1029/2005GL023740, 2005.
- Polyakov, I., Timokhov, L., Dmitrenko, I., Ivanov, V., Simmons, H., Beszczynska-Möller, A., Dickson, R., Fahrbach, E., Fortier, L., Gascard, J.-C., Hölemann, J., Holliday, N. P., Hansen, E., Mauritzen, C., Piechura, J., Pickart, R., Schauer, U., Walczowski, W., and Steele, M.: Observational program tracks Arctic Ocean transition to a warmer state, *Eos Trans. AGU*, 88(40), 398–399, <https://doi.org/10.1029/2007EO400002>, 2007.
- Polyakov, I. V., Alexeev, V. A., Ashik, I. M., Bacon, S., Beszczynska-Möller, A., Carmack, E. C., Dmitrenko, I. A., Fortier, L., Gascard, J.-C., Hansen, E., Hölemann, J., Ivanov, V. V., Kikuchi, T., Kirillov, S., Lenn, Y.-D., McLaughlin, F. A., Piechura, J., Repina, I., Timokhov, L. A., Walczowski, W., and Woodgate, R.: Fate of Early 2000s Arctic Warm Water Pulse, *Bulletin of the American Meteorological Society*, 92(5), 561–566, doi: 10.1175/2010BAMS2921.1, 2011.

- Polyakov, I. V., Pnyushkov, A., Rember, R., Ivanov, V., Lenn, Y-D., Padman, L., and Carmack, E. C.: Mooring-based observations of the double-diffusive staircases over the Laptev Sea, *J. Phys. Oceanogr.*, 42, 95–109, doi: 10.1175/2011JPO4606.1, 2012.
- 770 Polyakov, I. V., Pnyushkov, A. V., Alkire, M. B., Ashik, I. M., Baumann, T. M., Carmack, E. C., Goszczko, I., Guthrie, J., Ivanov, V. V., Kanzow, T., Krishfield, R., Kwok, R., Sundfjord, A., Morison, J., Rember, R., and Yulin, A.: Greater role for Atlantic inflows on sea-ice loss in the Eurasian Basin of the Arctic Ocean, *Science*, 356, 285–291, <https://doi.org/10.1126/science.aai8204>, 2017.
- 775 Rudels, B.: On the mass balance of the polar ocean, with special emphasis on the Fram Strait, *Skr. Nor. Polarinst.*, 188, 1–53, 1987.
- Rudels, B., Jones, E. P., Anderson, L. G., and Kattner, G.: On the intermediate depth waters of the Arctic Ocean, in: *The Role of the Polar Oceans in Shaping the Global Climate*, edited by: Johannessen, O. M., Muench, R. D., and Overland, J. E., American Geophysical Union, 780 Washington, DC, 33–46, 1994.
- Rudels, B.: Aspects of Arctic oceanography, in *Physics of ice-covered seas*, vol. 2, edited by: Leppäranta, M., Univ. Press, Helsinki, 517–568, 1998.
- Rudels, B., Björk, G., Muench, R. D, and Schauer, U.: Double-diffusive layering in the Eurasian Basin of the Arctic Ocean, *J. Mar. Syst.*, 21(1–4), 3–27, doi: 10.1016/S0924-7963(99)00003-2, 1999.
- 785 Rudels, B., Jones, E. P., Schauer, U., and Eriksson, P.: Atlantic sources of the Arctic Ocean surface and halocline water, *Polar research*, 23(2), 181–208, doi: 10.1111/j.1751-8369.2004.tb00007.x, 2006.
- ~~Rudels, B., Kuzmina, N., Schauer, U., Stipa, T., and Zhurbas, V.: Double-diffusive convection and interleaving in the Arctic Ocean—Distribution and importance, *Geophysica*, 45(1–2), 199–213, 2009.~~
- 790 Rudels, B.: Arctic Ocean circulation, processes and water masses: A description of observations and ideas with focus on the period prior to the International Polar Year 2007–2009, *Progress in Oceanography*, 132, 22–67, doi: 10.1016/j.pocean.2013.11.006, 2015.
- 795 Rudels, B., Korhonen, M., Schauer, U., Pisarev, S., Rabe, B., and Wisotzki A.: Circulation and transformation of Atlantic water in the Eurasian Basin and the contribution of the Fram Strait inflow branch to the Arctic Ocean heat budget, *Progress in Oceanography*, 132, 128–152, doi: 10.1016/j.pocean.2014.04.003, 2015.
- Schauer, U., Muench, R. D., Rudels, B., and Timokhov, L.: Impact of eastern Arctic shelf waters 800 on the Nansen Basin intermediate layers, *J. Geophysical Res.*, 102(C2), 3371–3382, 1997.

- Schauer, U., Loeng, H., Rudels, B., Ozhigin, V. K., and Dieck, W.: Atlantic Water flow through the Barents and Kara Seas, *Deep-Sea Res. Pt. I*, 49(12), 2281–2298, [https://doi.org/10.1016/S0967-0637\(02\)00125-5](https://doi.org/10.1016/S0967-0637(02)00125-5), 2002a.
- 805 Schauer, U., Rudels, B., Jones, E. P., Anderson, L. G., Muench, R. D., Björk, G., Swift, J. H., Ivanov, V., and Larsson, A.-M.: Confluence and redistribution of Atlantic water in the Nansen, Amundsen and Makarov basins, *Ann. Geophys.*, 20, 257–273, doi: 10.5194/angeo-20-257-2002, 2002b.
- Schauer, U., Fahrbach, E., Osterhus, S., and Rohardt, G.: Arctic warming through the Fram Strait: Oceanic heat transport from 3 years of measurements, *J. Geophysical Res.*, 810 109(C06026), doi: 10.1029/2003JC001823, 2004.
- ~~Stern, M. E.: Lateral mixing of water masses, *Deep-Sea Res.*, 14, 747–753, doi:10.1016/S0011-7471(67)80011-1, 1967.~~
- Swift, J. H., Jones, E. P., Aagaard, K., Carmack, E. C., Hingston, M., MacDonald, R. W., McLaughlin, F. A., Perkin, R. G.: Waters of the Makarov and Canada basins, *Deep-Sea Res.* 815 II, 44(8), 1503-1529, doi: 10.1016/S0967-0645(97)00055-6, 1997.
- Våge, K., Pickart, R. S., Pavlov, V., Lin, P., Torres, D. J., Ingvaldsen, R., Sundfjord, A., and Proshutinsky, A.: The Atlantic Water boundary current in the Nansen Basin: Transport and mechanisms of lateral exchange, *J. Geophys. Res.*, 121, 6946–6960, <https://doi.org/10.1002/2016JC011715>, 2016.
- 820 ~~Walsh, D., and Carmack, E.: The nested structure of Arctic thermohaline intrusions, *Ocean Model.*, 5, 267–289, doi: 10.1016/S1463-5003(02)00056-2, 2003.~~
- Walsh D., Polyakov I., Timokhov L., and Carmack E.: Thermohaline structure and variability in the eastern Nansen Basin as seen from historical data, *Journal of Marine Research*, 65, 685–714, 2007.
- 825 Woodgate, R. A., Aagaard, K., Muench, R. D., Gunn, J., Bjork, G., B. Rudels, Roach, A. T., and Schauer, U.: The Arctic Ocean boundary current along the Eurasian slope and the adjacent Lomonosov Ridge: Water mass properties, transports and transformations from moored instruments, *Deep-Sea Res. Pt. I*, 48(8), 1757–1792, [https://doi.org/10.1016/S0967-0637\(00\)00091-1](https://doi.org/10.1016/S0967-0637(00)00091-1), 2001.
- 830 ~~Zhurbas, N. V.: On the eigenvalue spectra for a model problem describing formation of the large-scale intrusions in the Arctic Basin, *Fundamentalnaya i Prikladnaya Gidrofizika*, 11(1), 40–45, doi: 10.7868/S2073667318010045, 2018.~~
- Zhurbas, N. V.: Estimates of transport and thermohaline characteristics of the Atlantic Water in the Eurasian Basin, *Russian Meteorology and Hydrology*, 44, 603–612, 835 doi: 10.3103/S1068373919090048, 2019

~~Zhurbas, V. M., Kuzmina, N. P., Ozmidov, R. V., Golenko, N. N., and Paka, V. T.:
Manifestation of subduction in thermohaline fields of vertical fine structure and horizontal
mesostructure in frontal zone of Azores Current, Okeanologiya, 33, 321–326, 1993.~~

840 ~~Zhurbas, V., Elken, J., Paka, V., Piechura, J., Väli, G., Chubarenko, I., Golenko, N., and
Shehuka, S.: Structure of unsteady overflow in the Slupsk Furrow of the Baltic Sea, J.
Geophys. Res.—Oceans, 117, C04027, doi:10.1029/2011JC007284, 2012.~~